Nihon Reoroji Gakkaishi Vol.51, No.5, 295~316
(Journal of the Society of Rheology, Japan)

DOI: 10.1678/rheology.51.295

Review

Rheology for Safe Swallowing 2‡

Katsuyoshi Nishinari[1, 18, †], Ke Zhang[1], Nan Yang[1], Zhiming Gao[1], Chaiwut Gamonpilas[2], Mihaela Turcanu[3], Marie-Agnès Peyron[4], Yapeng Fang[5], Yoko Nitta[6], Xiaolin Yao[7], Meng Zhao[8], Sayaka Ishihara[9], Makoto Nakauma[9], Takahiro Funami[9], Kaoru Kohyama[10], Hatsue Moritaka[11], Miki Yoshimura[12], Makoto Takemasa[13], Kazuhiro Hori[14], Koichiro Matsuo[15], Yukihiro Michiwaki[16], Yin Zhang[17], Narpinder Singh[18], and Aaron Goh Suk Meng[19]

[1] *Glyn O. Phillips Hydrocolloids Research Centre, Hubei University of Technology, Wuhan, 430068, China*
[2] *Advanced Polymer Technology Research Group, National Metal and Materials Technology Center (MTEC), NSTDA, 111 Thailand Science Park, Paholyothin Road, Khlong 1, Khlong Luang, Pathumthani 12120, Thailand*
[3] *Product and Process Engineering Center, Fresenius Kabi Deutschland GmbH, Daimlerstrasse 22, 61352 Bad Homburg, Germany*
[4] *Université Clermont Auvergne, INRA, UNH, Unité de Nutrition Humaine, CRNH Auvergne, F-63000, Clermont-Ferrand, France*
[5] *Department of Food Science and Technology, School of Agriculture and Biology, Shanghai Jiao Tong University, Shanghai 200240, China*
[6] *Natural Science Division, Ochanomizu University, 2-1-1 Otsuka, Bunkyo-ku, Tokyo, 112-8610, Japan*
[7] *School of Food and Biological Engineering, Shaanxi University of Science and Technology, Xi'an, Shaanxi 710021, PR China*
[8] *State Key Laboratory of Biobased Material and Green Papermaking, School of Food Science and Technology, Qilu University of Technology, Shandong Academy of Sciences, Jinan, 250353, China*
[9] *San-Ei Gen F.F.I., Inc., 1-1-11, Sanwa-cho, Toyonaka, Osaka 561-8588, Japan*
[10] *Institute of Food Research, NARO, 2-1-12, Kannondai, Tsukuba, Ibaraki, 305-8642, Japan*
[11] *Institute of Women's Health Sciences, Showa Women's University, 1-7-57, Taishido, Setagaya-ku, Tokyo, 154-8533, Japan*
[12] *School of Human Science and Environment, University of Hyogo, 1-1-12, Shinzaike-Honcho, Himeji 670-0092, Japan*
[13] *Division of Life Science and Engineering, School of Science and Engineering, Tokyo Denki University, Ishizaka, Hatoyama-cho, Hiki-gun, Saitama, 351-0394, Japan*
[14] *Division of Comprehensive Prosthodontics, Niigata University Graduate School of Medical and Dental Sciences, 2-5274 Gakkocho-dori, Niigata, Niigata, 951-8514, Japan*
[15] *Department of Oral Health Sciences for Community Welfare, Graduate School of Medical and Dental Sciences, Tokyo Medical and Dental University, 1-5-45, Yushima, Bunkyo-ku, Tokyo 113-8549, Japan*
[16] *Department of Oral Surgery, School of Medicine, Toho University, Tokyo 143-8541, Japan*
[17] *Key Laboratory of Meat Processing of Sichuan, Chengdu University, Chengdu 610106, China.*
[18] *Department of Food Science and Technology, Graphic Era Deemed to be University, Dehradun-248002, Uttarakhand, India*
[19] *Engineering Cluster, Singapore Institute of Technology, 10 Dover Drive, 138683, Singapore*
(Received : May 31, 2023)

Key Words: Bolus / Mastication / Yield stress / Aspiration / Cohesive

6. EATING DIFFICULTY

Takahashi and Nakazawa[141] introduced a method to examine the chewing behaviour: a small pressure transducer was inserted into an artificial tooth to record the force from the first bite until the stage of swallowing without interfering with the normal occlusion of the teeth. Although this method is useful to quantify the chewing activity, it cannot be used for persons with all his/her own teeth.

Eating difficulties were classified according to the symptoms and possible causes (Table VI).

Sensory evaluation is useful for this problem. Chen and Lolivret[100] categorized the eating difficulty based on the residence time of ingested food. Their panelists were instructed to judge the eating difficulty by the length of residence time as mentioned above[174].

Hayakawa *et al.*[175] examined the eating difficulty using twenty model food gels, such as ι-carrageenan, κ-carrageenan, mixture of κ-carrageenan and locust bean gum (LBG), low acyl gellan, low methoxyl pectin, mixture of LBG and xanthan (XG), gelatin, agar, high acyl gellan. These model gels have a wide range of textural characteristics, firmness,

† Corresponding author.
E-mail : katsuyoshi.nishinari@gmail.com
‡ Editorial notes: This review article is the second in a three-part serial[174].

Table VI Eating difficulties of elderly people, possible causes and suggested solutions[173].

Symptoms	Possible causes	Suggested non-medical solutions
Chewing difficulty	Lack of functional teeth Reduced tongue & jaw muscles Reduced bite force	Size reduction of food Texturally modified food
Dry mouth	Lack of saliva secretion Reduced saliva flow rate Open mouth respiration	Artificial saliva application Moisturized/liquidized food Saliva stimulation (physically and bio-chemically)
Oral manipulation difficulty	Reduced lip sealing pressure Reduced tongue muscle strength Reduced touching sensitivity (tactile)	Size reduction of food Texturally modified food
Tasting difficulty	Dry mouth Reduced saliva secretion Change of saliva composition	Artificial saliva application Addition of flavoring compounds in food
Swallow difficulty	Tongue displacement Reduced muscle activities	Texturally modified food
Aspiration or suffocation	Reduced laryngeal movement	Increase in oral transit duration Thickened liquid intake (rather than thin liquid intake)
Choking	Insufficiently processed food intake Reduced laryngeal muscles	Texturally modified food
Loss of appetite	Dry mouth or tasteless	Orally and aromatically multi-stimulation

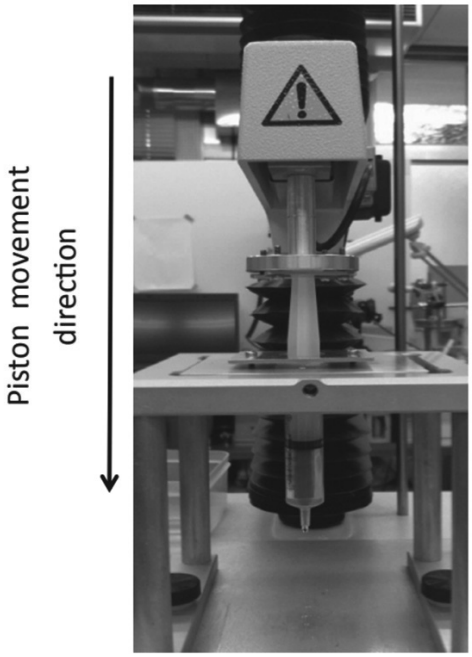

Fig. 41 Experimental setup for extrusion test. A syringe is pushed down by a plunger of a texture analyser[41].

cutting effort, elasticity, extensibility, adhesiveness, melting rate in the mouth, and eating difficulty. Based on principal component analysis, they concluded that resistance to fracture and stickiness and flexibility are critical eating difficulty factors. Gelatin-based gels are perceived as less firm and less hard than expected based on their mechanical properties compared to polysaccharide gels that have the same mechanical properties at room temperature but melt well above body temperature, underlying the importance of the measurement temperature for gels that melt during mastication.

Eating difficulty of gels of 5 % gelatin and its mixture with konjac glucomannan (KGM) (0.5, 1, 2 %) and LBG (0.5, 1, 2 %) were studied and compared with rheological properties by Tomczynska-Mleko *et al.*[176]. Eating difficulty was rated as follows: Hardness (+2 very hard, +1, 0, −1, −2 very soft); Difficulty of chewing (+2 very difficult, +1, 0, −1, −2 very easy); Slipperiness or stickiness (+2 very slippery, +1, 0, −1, −2 very sticky); Difficulty of swallowing (+2 very difficult, +1, 0, −1, −2 very easy). Panelists judged gels with high content of LBG difficult to chew and swallow because these gels were perceived sticky. Sticky gels stick to the teeth and the hard palate, and thus could not be located at the right position to be fractured. Eating difficulty of gelatin/KGM (konjac glucomannan) mixed gels was studied by the same group[177] who found that these mixed gels in the presence of sucrose maintaining the melt-in-mouth showed no difficulty although the mixed gels without sucrose showed the difficulty caused by the increase in stickiness with increasing KGM.

Brenner *et al.*[41] studied the correlation between the extrusion force of the same polysaccharide gels except gelatin gels used in the study of Hayakawa *et al.*[175] with a syringe shown in Fig. 41 not exactly the same as used in IDDSI (The International Dysphagia Diet Standardisation Initiative) extrusion and the sensation of difficulty in swallowing.

Brenner *et al.*[41] expected that oral perception will correlate better with extrusion, a large deformation process involving both normal (extensional) and shear deformations, than it does with a conventional and instrumental texture profile analysis (TPA), which usually involves only uniaxial compression. Brenner *et al.*[41] tried to find a correlation between the sensory evaluated firmness, cutting effort, extensibility with instrumentally measured TPA engineering fracture stress, TPA engineering fracture strain, TPA 90 %-strain engineering stress, TPA cohesiveness, storage Young's modulus, maximum extrusion pressure from the syringe, extension fracture stress from ring extension, extension fracture strain from ring extension, normalized displacement to penetration, puncture fracture stress. Taking into account that human perception must saturate at very high stimuli, and not be present at physical stimuli below the sensitivity threshold, the sensory score "*S*" could be assumed to be a sigmoid function

$$S = A_{\min} + \frac{A_{\max} - A_{\min}}{1 + \exp\left(C_1 + C_2 X\right)} \tag{1}$$

where X is a physical property, C_1 and C_2 are fit parameters, and $A_{\min}$ and $A_{\max}$ are the minimum and maximum scores of

Table VII Parameters used for correlation analysis[41].

Parameter	Symbol	Test	Definition
Engineering fracture stress	σf	TPA	Force/initial sample area at first visible peak; equal to $\sigma 90$ for samples that do not fracture
Engineering fracture strain	γf	TPA	Distance/initial height of at first visible peak; equal to 0.9 for samples that do not fracture
90% engineering stress	$\sigma 90$	TPA	Force/initial sample area at 90% compression
Cohesiveness	C	TPA	Ratio of energy in second and first compression cycles
Storage Young's modulus	E	Rheolograph	Ratio of extensional stress and strain in viscoelastic linear regime
Maximum extrusion pressure	P_{max}	Extrusion	Maximum force in extrusion divided with cross-section of syringe, evaluated for different experimental setups
Extrudability	EX	Calculated	$\ln(E/P)$, evaluated for different experimental setups
Firmness	F	Sensory evaluation	Force required to slightly deform the sample between tongue and palate
Cutting effort	CE	Sensory evaluation	Force needed to achieve fracture by chewing once between the molars
Extensibility	D	Sensory evaluation	Degree to which the sample could be deformed without fracture between tongue and palate
Extension fracture strain	$\gamma f(e)$	Ring extension test	Engineering fracture strain at ring fracture
Extension fracture stress	$\sigma f(e)$	Ring extension test	Engineering fracture stress at ring fracture
Normalized displacement to penetration	$\gamma f(p)$	Puncture test	Distance to fracture divided with initial sample height
Puncture fracture stress	$\sigma f(p)$	Puncture test	Engineering fracture stress

the sensory score scale, respectively. Combining this type of equation, the high correlation was found; the ratio of the extrusion force (stress) to the Young's modulus correlated highly with the sensory extensibility; and a logarithmically weighted average of the extrusion force (stress) and the Young's modulus correlated highly with the sensory firmness. Since these results were obtained for a wide range of the texture from very brittle to very ductile, further development is expected. Brenner, Tomczynska-Mleko, Mleko & Nishinari[178] found that gelatin gels deviated from such a good fit obtained for polysaccharide gels at room temperature, and attributed it to the lower melting temperature of gelatin; the correlations, obtained using instrumental tests performed at a temperature far below body temperature, are not valid when the texture is strongly temperature-dependent over the temperature range covering the body and test temperatures. This is in line with Clark[179] (2002) and Bayarri, Rivas, Costell, & Duran[180] who reported higher sweetness intensity or higher diffusion coefficient of sweeteners in gels with lower melting temperatures. The sensory cutting effort (close to the widely used definition of sensory hardness) and extensibility (the degree to which the food can be deformed without fracture) were found well predicted by instrumental parameters from the extrusion test for gels containing kappa- and iota- carrageenans, KGM and XG[178].

Another slip extrusion test (SET) in which the foods with wide range of texture were extruded in the nylon-polyethylene bag (70 microns thick) by peristalsis and flow driven by pulling the bag through the two rollers[183]. Peristalsis of boli by two rollers was also used[181] and further developed by the same group to take into account the wettability and deformability of the pharyngeal mucosa[182].

In the SET test[183], foods were moved from a wider part to a narrower one of the bag, and the resistance to deformation and the resistance to slip were recorded. Ng *et al.*[182] claimed that this SET could measure the rheological properties with wide range; xanthan solutions (1–2 %w/w), glass beads ballotini dispersed in 0.1 % xanthan, where xanthan solution in mixture ranged from 0 to 50 %, gelatin cuboid gels containing sugars, and citric acid with different hardness. Deformation resistance and slip resistance were measured for these model foods as a function of viscosity for xanthan solutions, hardness for gelatin gels, xanthan sol content in glass ballotini dispersion. Further, deformation resistance and slip resistance for peanut boluses with different number of chews were measured. The authors are trying to establish the criteria for a safe to swallow bolus based on SET.

It was shown that xanthan solutions displayed the most suitable oral cohesiveness relative to their perceived oral propulsion effort, stickiness, and oral residue compared to starch

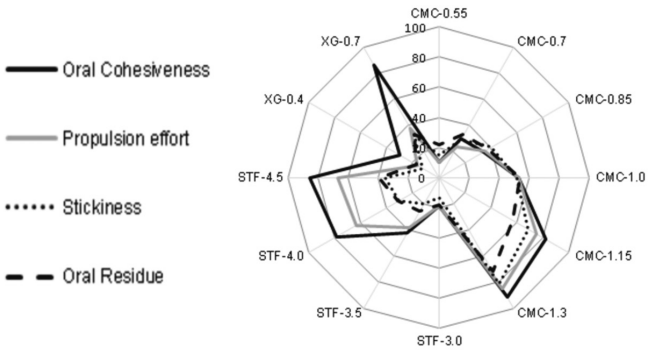

Fig. 42 Average scores of sensory attributes for all thickened fluid samples on 0-100 anchored sliding scale (0 = least intense, 100 = most intense). XG-0.4, xanthan gum 0.4 %w/v; STF-4.0, modified tapioca starch ST(modified tapioca starch) used in the text[184] as confirmed by Ross.

or carboxymethyl-cellulose solutions[184] (Fig. 42). Highly shear-thinning fluids with a yield stress are expected to have beneficial flow properties when used as therapeutic interventions to improve swallowing safety and efficiency in consumers with dysphagia.

Oral cohesiveness, propulsion effort, stickiness, and oral residue were defined in Table VIII[184].

These are consistent with previous findings[67] that xanthan solutions were more cohesive with higher yield stress than locust bean gum solutions, and attributed this to the smaller internal binding force in locust bean gum due to the lack of the intermolecular associations, leading to the absence of ordered structure and to decreased score of sensory cohesiveness. Nakauma *et al.*[67] showed that mechanical cohesiveness is a synonym of the internal binding force that contributes to the formation of one coherent bolus[38]. Sensory evaluations[67] corroborated the acoustic measurements of the swallowing process.

It was shown that highly shear-thinning fluids such as xanthan gum solutions had lower intensities of perceived stickiness, adhesiveness and mouth coating, and the smaller residue sensation after swallow based on the comparison of fifteen different hydrocolloids[111]. It was also found that concentrated xanthan solutions displayed greater slipperiness than less shear thinning guar gum and carboxymethyl cellulose solutions when fluids are squeezed between the tongue and the hard palate[185]. The slipperiness of xanthan solutions was pointed out as mentioned above in relation with Fig. 24 showing the flow velocity and shear rate in the syringe barrel and at the nozzle-end orifice[110].

As mentioned before on the timing of swallow[51], the identification of the time at which the cohesiveness becomes maximum poses some questions. From the viewpoint of difficulty for oral processing, liquids with low viscosity seem to be easier to be swallowed. The hypothesis of the maximum cohesiveness for the triggering of swallowing was questioned because swallowing muscle is required to work harder to transport the bolus to the posterior region of oropharynx[100]. In this study[100], the oral residence time of 28 fluid foods with varying viscosities from 0.001 to 100 Pas at the shear rate from 1 to 100 s^{-1}, were evaluated by 19 panelists (average 29 years old). It was shown that the liquids with low viscosity showed a shorter residence time in the oral cavity, indicating that thicker boli were perceived difficult to be swallowed. Chen *et al.*[100] thought that appropriate flow-ability is required for triggering swallow. Although the sensory difficulty of swallowing and the shear viscosity are positively correlated, a better correlation between the sensory difficulty of swallowing and the force or the work of fluid stretching was found[100]. It was believed reasonable because the length of the bolus was increased, highly stretched and extensional deformation became dominant in the pharyngeal phase though shear deformation was dominant in the oral phase[186].

A simultaneous measurement to evaluate the eating difficulty of two gruel samples, *zengayu* (common gruel) and *fukkuraokayu* (less adhesive/sticky gruel) was performed[187]. Six healthy panelists evaluated these two gruel samples, each 5 g gruel at 60 °C. Larynx motion was found faster in the early phase of swallowing of *fukkuraokayu,* and suprahyoid musculature was found less active for swallowing of *fukkuraokayu.* These findings suggested that *fukkuraokayu* could be swallowed more easily than common gruel.

Sticky rice cake (*mochi*) made from glutinous rice is known to be difficult to bite it off and causes sometimes choking accidents, and has been causing death in elderly or children in Japan. Therefore, texture-modified rice cakes are produced adding non-glutinous rice flour or high amylose starch. Simultaneous measurement mentioned above was ap-

Table VIII Sensory attribute descriptions and assessment methods used by the trained sensory panel, and their relevance to common swallowing impairments[184].

Sensory attribute name	Assessment definition	Assessment method {Descriptor anchors for 0–100}	Relevance to swallowing impairments
Oral cohesiveness	How well the bolus holds together on the tongue	Place 1 spoonful (2.5 mL) of sample onto your tongue and hold for a maximum of 4 s; maintain an upright posture with level chin and relaxed tongue. Assess cohesiveness. {None-High}	Impaired oral manipulation
Propulsion effort	The ability of the tongue to move the bolus in order to initiate the swallow	Move the bolus toward the back of the tongue and then initiate the swallow. Assess propulsion effort. {Requires little effort - requires great effort}	Impaired oral propulsion
Stickiness	Stickiness of the sample when depressed between the tongue and roof of mouth and then swallowed; felt in the oral cavity, tongue and/or lips	Place an additional 1 spoonful (2.5 mL) onto your tongue and depress between roof of mouth and tongue, then swallow. Assess stickiness. {None-High}	Impaired oral clearance
Oral residue	Amount of residue detected in the mouth after swallowing	Following swallow from stickiness assessment, assess oral residue. {None-High}	Impaired oral clearance

plied to rice cake as shown in Fig. 43[188].

Kohyama *et al.*[188] interpreted these detected signals as follows: suprahyoid musculature, swallowing sound, and the upper and middle pressure sensors (the upper sensor 3 and the middle sensor 2 in Fig. 40c[157] (Part 1 of the this review)) showed no signals before swallowing, but the lowest pressure sensor (the lower sensor 1 in Fig. 40c) exhibited a positive pressure because it was pressed by the mound of the thyroid cartilage. After the commencement of swallowing, suprahyoid electromyography (SH EMG) began to appear, caused by the tongue motion moving the bolus from the oral cavity to the oropharynx. Then, the pressure detected at the lower sensor 1 decreased, and the pressure at the middle sensor 2 and the sensor 3 increased to show a peak. This sequence corresponded to the elevation of the larynx. After the swallowing which was seen by the disappearance of the sound and SH EMG activity, the upper sensor 3 and the middle sensor 2 showed the second peak respectively, and the lower sensor 1 was found to increase again to the initial level. Kohyama *et al.*[188] compared the mastication behaviour for sticky rice cake and a modified rice cake, *Yawaraka Fukumochi* made from non-glutinous rice, with a lower firmness and a higher water content. They reported that the number of chewing and mastication time were smaller in 3 g than 9 g amount and similar between 3 g of standard rice cake and 9 g of *Yawaraka Fukumochi*, but SH EMG amplitude during mastication was lower in 3 times the amount of *Yawaraka Fukumochi*. The swallowing parameters, SH EMG amplitude and activity, swallowing sound, upper and middle pressure sensor, swallowing period were not significantly different in both types of rice cakes. Since their subjects were 11 healthy persons, it was suggested that the swallowing was induced when the bolus properties were perceived suitable for swallowing as the healthy subjects could adjust their mastication behaviour when the food amount and the properties were changed[188]. Since it is dangerous to use disadvantaged panelists, it is not possible to conclude that the above mentioned *Yawaraka Fukumochi* is safe for frail persons, but quantitative measurements based on SH EMG have never been done before.

A light and flexible motion sensor (Fig. 44) detecting the laryngeal movement during swallowing was fixed on the larynx which did not inhibit the natural eating[189]. Laryngeal movement was monitored by tracing the thyroid cartilage (so-called Adam's apple). Li *et al.*[189] identified 7 time points in the electric waveform and its first and second derivative from the comparison with the simultaneously observed videofluorograph (VF).

Combining EMG during squeezing model soft gels between the tongue and the hard palate and acoustic analysis of swallowing sound, Funami *et al.*[190] discussed the eating difficulty could be evaluated in conjunction with sensory analysis. The thyroid cartilage movement during swallowing of thickened liquids was monitored[191] using a bendable pressure sensor synchronously with suprahyoid electromyography, and the relation between this thyroid cartilage movement and the sensory evaluation was examined. The negative correlation between the thyroid cartilage movement and the cohesiveness of liquids was found because more coherent liquids required less activity of thyroid cartilage. It is also consistent with findings that the shorter time required for bolus to transfer through the pharynx corresponded to the perceived swallowing ease, in line with Fig. 28c[66, 67] (Part 1 of this review). The shorter time for passage was attributed to one coherent flow of bolus during swallowing[67].

This method was applied to examine the relation between texture sensation with laryngeal movement in swallowing[192].

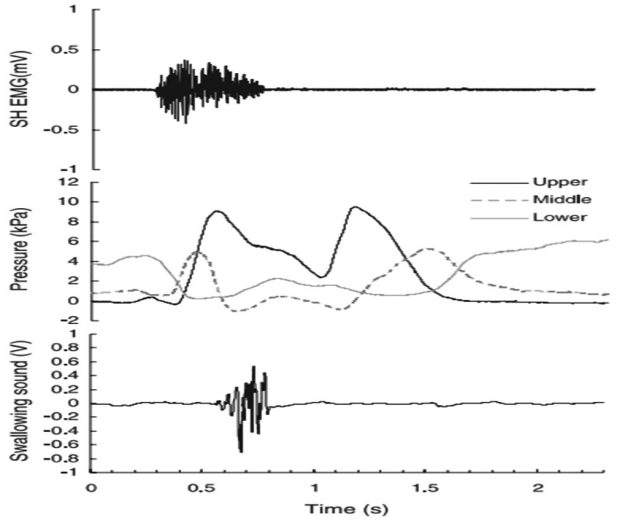

Fig. 43 Typical swallowing recordings for a sticky rice cake (9 g). Upper figure, electromyographic (EMG) activity of suprahyoid (SH) muscle; middle, pressure detected by sensors installed at upper, middle and lower region at thyroid cartilage; lower, swallowing sound[188].

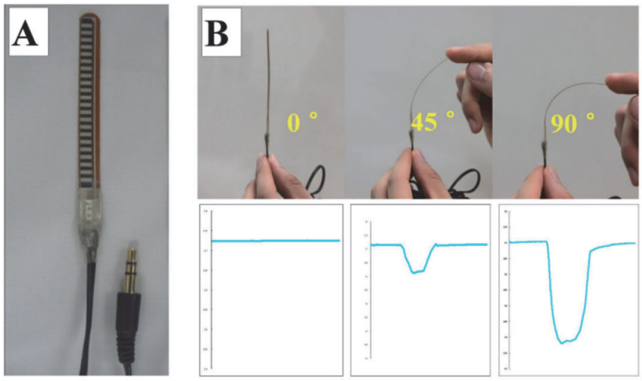

Fig. 44 Bend senor detecting the laryngeal movement. A) A thin flexible membrane, B) Electric resistance changes with mechanical deformation (bending). This change is larger for larger bending angle[189].

Figure 45 shows the laryngeal movement, suprahyoid musculature activity, and tongue activity during water swallowing.

Nine boluses made from polysaccharide gels with different rheological properties were used[192]. All 9 boluses consisted of ca 370 small cubic gels (each 3 mm × 3 mm × 3 mm) equivalent to the mass of 10 g, which was served by a spoon into the mouth of 9 male subjects (average 30 years old) by an experimenter. Subjects were instructed to hold the bolus in the oral cavity for 3 s, and then swallow at one time without chewing and to score hardness, bolus uniformity, and swallowing ease as textural perception during swallowing on the Visual Analog Scale (VAS). Since the thyroid cartilage or hyoid movement in female subjects was difficult to detect, subjects were limited to male. Since the same research group reported that the average size of particle in bolus just before swallowing was 1.34 mm × 1.34 mm × 1.34 mm[193], they tried to make the model bolus consisting of the cubic gel (1.34 mm × 1.34 mm × 1.34 mm), but it was difficult and the bolus consisting of 370 small cubic gels (each 3 mm × 3 mm × 3 mm) was used[192]. In addition, this size has been a matter of debate for a long time. It has been generally accepted that particle size in the bolus just before swallowing was larger for soft and deformable particles than for harder and non-deformable ones as mentioned before[38, 125].

In the sensory evaluation, the hardness was related to the texture perception caused by the contact between the small cubic gels and the pharynx during swallowing while the instrumental hardness (TPA hardness) was determined at 90 % compression. TPA hardness can be associated with the stress produced at the inner pharynx wall when the bolus passes through the stenosis of the pharyngeal phase during swallowing, thus resulted in high correlation with perceived hardness. TPA hardness for the model boluses was found to increase as the fracture force increased when compared among the gel samples of equivalent fracture strain, while apparent tendency was not observed for either TPA adhesiveness or TPA cohesiveness.

Among all the variables, the highest correlation with perceived hardness was found in the suprahyoid musculature activity detected by EMG, whereas the highest correlation with perceived bolus uniformity and with perceived swallowing ease was found in the duration of swallowing (T2 to T6 in the laryngeal movement) and in the tongue activity (from tongue pressure measurement), respectively. These 3 variables showed relatively high correlation with all textural perception.

7. VISCOSITY IN THE SWALLOWING

Let's examine the role of the liquid viscosity in the

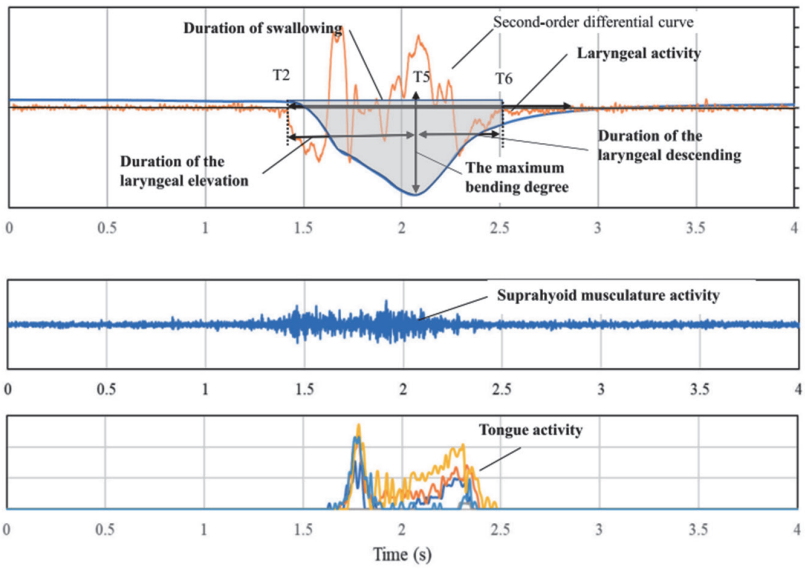

Fig. 45 Waveform from synchronous measurements of the laryngeal movement monitored by bending sensor shown in Fig. 44, suprahyoid muscular activity detected by EMG, and tongue pressure detected by a sensor sheet shown in Fig. 35 (Part 1 of this review) during human swallowing of water (10 g) at one time. The time point at which the second-order differential curve (acceleration) deviates from the baseline (*i.e.* the point at which the larynx begins to accelerate upward) is defined as T2, and the time point at which the second-order differential curve converges on the baseline (*i.e.* the point at which the accelerated descent of the larynx ends) was defined as T6. For the laryngeal movement, the time from T2 to T6 was defined as the duration of swallowing. The difference in the signal from the baseline of the signal waveform to the maximum descent point (T5) was defined as the maximum bending degree of the sensor, the time from T2 to T5 as the duration of the laryngeal elevation, the time from T5 to T6 as the duration of the laryngeal descending, and the area of the signal waveform during the duration of swallowing (from T2 to T6) as the laryngeal activity[192].

swallowing again. As mentioned above, the risk of aspiration could be reduced by increasing the viscosity. However, excessive thickening reduces the palatability and the intake of fluids leading to dehydration and malnutrition[194, 195]. In addition, the excessive thickening may form residues[26, 196, 197] at the epiglottis vallecula or pyriform sinus, which subsequently may cause the aspiration. In addition, the excessive thickening may cause choking as in the rice cake or konjac jellies as discussed earlier in the introduction.

Effects of viscosity of gums/starch thickener on the safety and efficacy of swallow are shown in Fig. 46 for four different subject groups; older, head and neck cancer (HNC), Parkinson's disease, chronic post stroke.

The upper figure shows that the probability of safe swallow increased with increasing viscosity of the thickeners consisting of xanthan gum and modified starch. The minimum viscosity tested (250 mPas) showed a significant therapeutic effect vs. thin liquid for all the four groups studied and it increased until the maximum viscosity assessed (2000 mPas) achieving higher than 90 % of safe swallows in older, Parkinson's and stroke groups and 75 % in head and neck cancer patients. However, no significant differences were seen between 1000 mPas and 2000 mPas for each group compared individually. Therefore, the threshold viscosity of safety was 250 mPas, and maximal viscosity was 1000 mPas. In other words, it is necessary to increase the viscosity at least above 250 mPas, and it was not effective to increase the viscosity further above 1000 mPas. Head and neck cancer group showed the worst achievement[198].

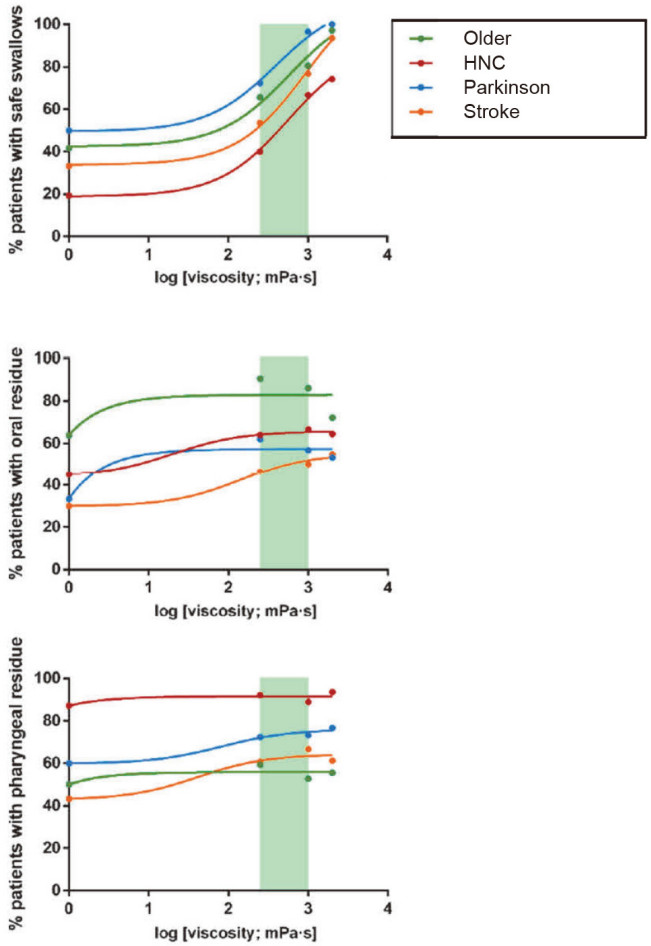

Fig. 46 Percentage of patients who could swallow safely (upper), percentage of patients with oral residue (middle), percentage of patients with pharyngeal residue (lower) as a function of the viscosity of thickeners[198].

The middle and the lower figure of Fig. 46 show the probability of residues remained in the oral region and pharyngeal region, respectively. Again, the head and neck cancer group showed the worst achievement: the pharyngeal residue was highest among the four groups.

Figure 47 shows the shear rate dependence of three thickener solutions of xanthan gum and guar gum with different molar masses[199]. Lower molar mass guar gum solution showed a Newtonian plateau at lower shear rates while xanthan gum solution shows a shear thinning behavior as has been reported by many research groups. The apparent shear thickening found in a xanthan solution was not found when the shear rate was decreased from 1000 to 0.03 s^{-1} as was shown in Fig. 4 of the paper[199]. Three solutions were prepared so that the viscosity shows the same value at the shear rate 50 s^{-1}, which is widely used as the shear rate in the oral cavity although the complete consensus was not reached[200].

Figure 48a shows a videofluorograph (VF) for a patient who aspirated all the three solutions. Although all the three

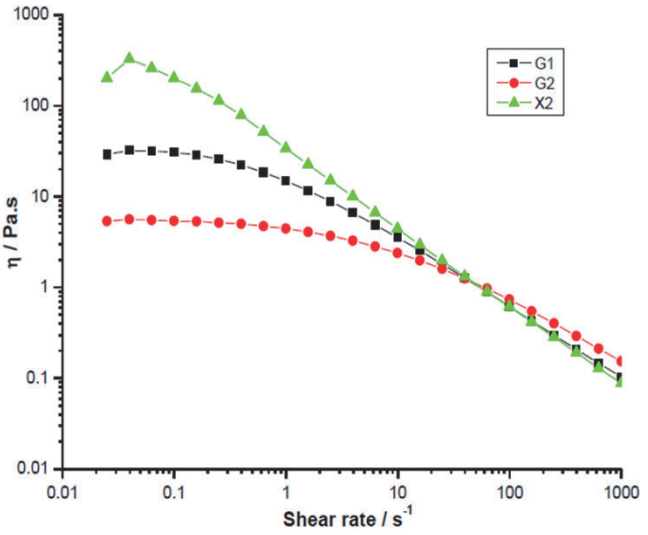

Fig. 47 Sher rate dependence of the viscosity for Sample 1 (G1, black square), 2.0 wt % guar gum solution stirred at room temperature for 10 h, then heated at 75 °C for 1 h; Sample 2 (G2, red circle), 2.6 wt% guar gum solution stirred at room temperature for 10 h, then heated at 75 °C for 1 h and sterilized at 121 °C for 20 min. Sample 3 (X2, green triangle), 4.1 wt% xanthan solution stirred at room temperature for 10 h, then heated at 75 °C for 1 h and sterilized at 121 °C for 20 min[199].

solutions were aspirated, the amount of the aspiration was the lowest for the xanthan solution.

Figure 48b shows VF for another patient. No aspiration was found in X2, which has the highest viscosity at lower shear rates. A huge amount of aspiration was observed for G1 and a moderate aspiration was observed for G2. Since $\eta(X2) > \eta(G1) > \eta(G2)$ at lower shear rates. It seems that the viscosity at lower shear rate is important. But, this explanation is not valid between the difference in G2 and G1, and further study is needed. One possible reason is that the high viscosity solution at lower shear rate is difficult to swallow when compared in the same guar solution, as has been commented by healthy subjects.

Figure 48c shows VF for another patient. No aspiration was observed in G1. Small amount of aspiration was observed for both G2 and X2. No reasonable explanation for this was found yet.

In summary, it was shown that the degree of aspiration depended on the degree of shear thinning of polysaccharide solutions. This study showed the possibility to find what kind of fluid induces the aspiration and to reduce the risk of aspiration in dysphagic patients by controlling the food rheology.

Analysis of the total 32 cases revealed that the ratio of aspiration was in the following order: X2 (▲): 4/32 < G1 (■): 5/32 < G2 (●): 7/32. Since the viscosity at lower shear rates were in the following order, $\eta(X2) > \eta(G1) > \eta(G2)$, the probability of the aspiration was found lower for the solution with a higher viscosity at lower shear rates.

However, if the solution with higher viscosity at lower shear rates was safer, the VF shown in Fig. 48b which showed a huge aspiration for G1 than for G2 could not be explained by this logic. Figure 48c showing no aspiration for G1 and a small aspiration for G2 and X2 also could not be explained in the same way. Further study is needed.

Microgels have been found versatile for rheological control of food[201-203]. Recently, the suitability of agar microgels was examined[204]. Zhang *et al.*[204] reported that the storage modulus was higher than the loss modulus at an angular frequency range from $\omega = 1$ to 100 rad/s and both moduli are increasing only slightly with increasing ω as is widely found for structured liquids (previously called weak gels) (Fig. 49). In addition, the slope of the double logarithmic plot of the modulus and ω was smaller for agarose microgels than for xanthan solutions indicating the former is more solid-like than the latter at the equivalent concentrations.

The value of moduli for agar microgels (2000 Pa for 1 % agar microgel) reported[204] was about four times larger than that for agarose microgels (500 Pa for 1 % agarose microgel) reported[205]. Lower moduli of agarose microgels reported by Ghebremedhin *et al.*[205] could probably be attributed to the slower cooling rate, longer shearing time at a higher shear rate in comparison with the production condition of Zhang *et al.*[204]. It should be also reminded that agaropectin does not necessarily lower the gelling ability of agarose when coexisting[206, 207].

Thus, agar microgels are expected to be useful for

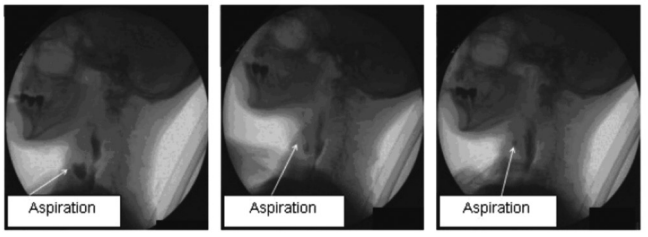

Fig. 48a Videofluorograph of a patient who aspirate all the three solutions[199].

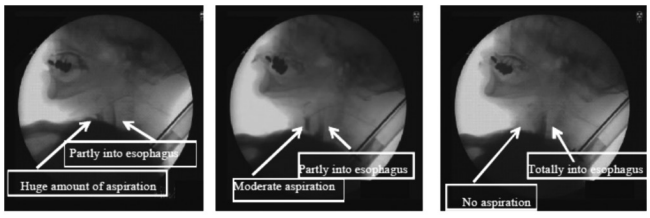

Fig. 48b Videofluorograph of a patient. No aspiration in X2, which has the highest viscosity at lower shear rates. $\eta(G2) > \eta(G1)$ at higher shear rates although $\eta(G2) < \eta(G1)$ at lower shear rates[199].

Fig. 48c Videofluorograph of a patient. No aspiration in X2, which has the highest viscosity at lower shear rates. $\eta(G2) > \eta(G1)$ at higher shear rates although $\eta(G2) < \eta(G1)$ at lower shear rates[199].

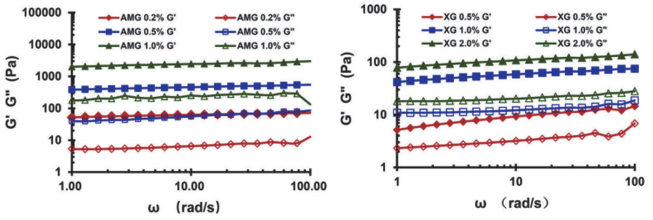

Fig. 49 Storage and loss moduli of agar microgel (AMG) with the concentrations (0.2 %, 0.5 %, and 1.0 %) (Left) and xanthan gum (XG) solutions with the concentrations (0.5 %, 1.0 %, and 2.0 %) (Right), as a function of angular frequency ω at constant stress 1 Pa and at 20 °C[204].

dysphagia diet because they showed quite a high modulus (Fig. 49) as well as yield tress (not shown here, see Fig. 2 of Zhang *et al.*[204]) than xanthan solutions at the same concentration although it is necessary to examine the effect of saliva on the cohesiveness, and the coexisting nutritional compounds. The efficacy of agar microgels is shown in Fig. 50.

Let us remind some fundamentals of viscosity of polymer solutions. Most liquid foods are non-Newtonian. The most commonly used models to represent the non-Newtonian fluid behaviour are power law, Bingham, Herschel-Bulkley (Fig. 51) and Casson.

It is necessary to take into account the shear rate dependence when we see the effect of viscosity. Figure 52 shows the viscosity of 2 % hydroxyethyl methylcellulose with different M_w in 0.01M $NaNO_3$ solution as a function of shear rate. The lower shear rate viscosity, called zero shear viscosity, increases with increasing molar mass of hydroxyethyl methylcellulose[210, 211].

Figure 53 shows the shear rate dependence of the steady shear viscosity of 0.5 % guar gum degraded by an enzyme β-mannanase. With increasing reaction time of enzymatic degradation, the polymer was degraded into a lower mass sample. Thus, this shows a similar tendency as the previous Fig. 52.

A Cross model is widely used to analyse such a shear rate dependence of polymer solution:

$$\frac{\eta - \eta_\infty}{\eta_0 - \eta_\infty} = \frac{1}{1 + (K\dot{\gamma})^m} \tag{2}$$

where, η_0 and η_∞ represent the viscosity at very low and very high shear rates respectively, K has the dimensions of time,

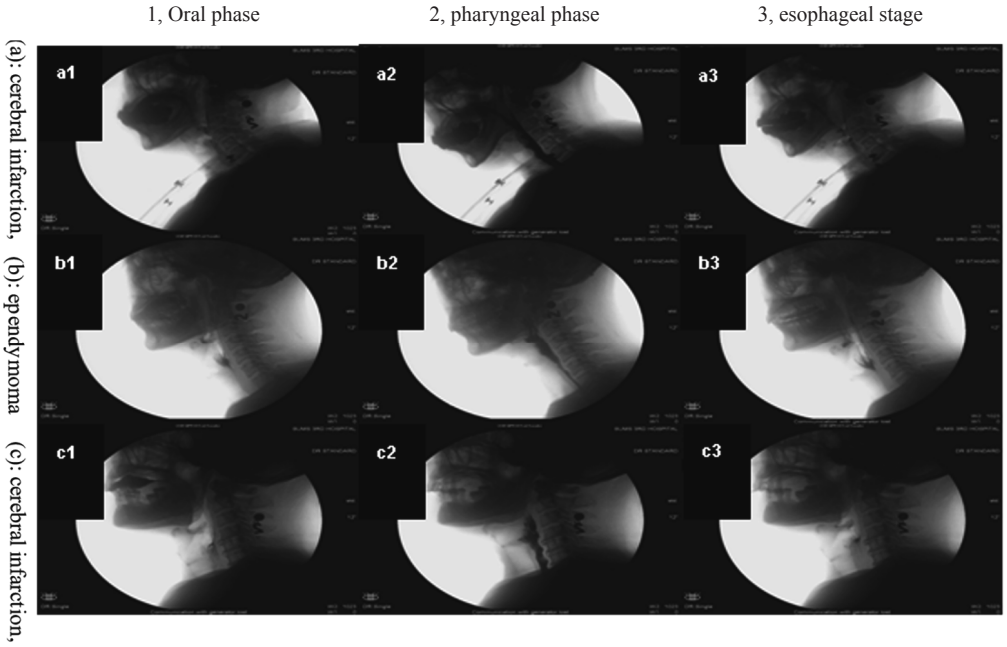

Fig. 50 VF images of swallowing agar microgel of patients suffering from three different diseases (a) cerebral infarction, (b) ependymoma, (c) cerebral infarction. Left to right numbers from 1 to 3 indicates three stages, 1, Oral phase; 2, pharyngeal phase; 3, esophageal stage. No aspiration was found in all three patients[204].

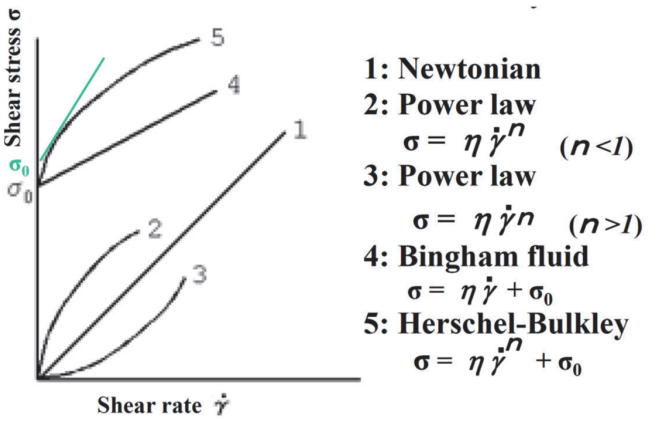

Fig. 51 Model flow curves commonly used to analyze the viscosity of various fluids. The yield stress determination depends on the drawing of the tangent as shown[208, 209].

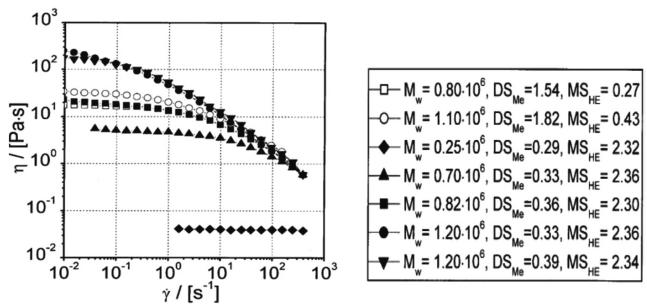

Fig. 52 Shear rate dependence of the viscosity of 2 % hydroxyethyl methylcellulose with different M_w in 0.01 M $NaNO_3$ solution[211].

and *m* is dimensionless. When this model is used to describe non-Newtonian liquids, the degree of shear thinning is dictated by the value of *m*, with *m* tending to zero describes more Newtonian liquids, while the most shear-thinning liquids have a value of *m* tending to unity[213].

Shear rate dependence of the viscosity of guar gum solutions with different concentrations was shown to fit well to the Cross model (Fig. 54).

Figure 55 shows the shear rate dependence of the viscosity for different thickened liquids at different levels of liquid consistency categorized by IDDSI viscosity level: (a) IDDSI level 1, (b) IDDSI level 2 and (c) IDDSI level 3. For each IDDSI, the concentration of each liquid was selected to have similar viscosity at shear rate 50 s^{-1}. The thickener solutions used are prepared from xanthan, maltodextrin, guar gum, tara gum etc. All these observed curves were fitted well by Cross model.

The relation between the perceived thickness *Th* and the instrumentally measured viscosity η_N has been studied extensively. For various Newtonian liquids such as syrup, honey and guar gum solutions, a linear relation between log *Th* and log η_N was found while that relation for "weak gels" (fluids with yield stress. The name "weak gels" was retracted later by one of namers) such as tomato ketchup and xanthan dispersions deviated from the linear relation and the perceived thickness *Th* was found lower than that for the other Newtonian fluids[216]. Morris[216] found a high correlation between *Th* and complex viscosity η^* at 50 rad s^{-1} and interpreted this result as *Th* was closely related with unbroken network characterized by η^* rather than η_N where the network was destroyed in making the measurement[216]. On the other hand, the possibility that sensory panelists may not swallow immediately when asked to evaluate the thickness as

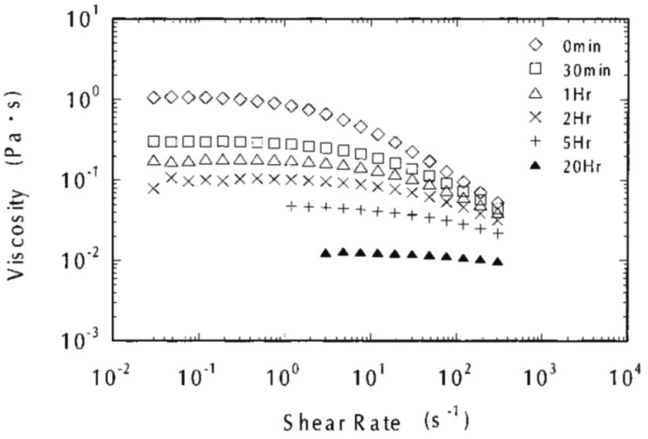

Fig. 53 Viscosity of 0.5 wt% guar solution as a function of shear rate plotted at different periods during enzymatic degradation. The reaction is run at ambient temperature and pH of 7. The concentration of β-mannanase is 0.0002 units/mL polymer solution[212].

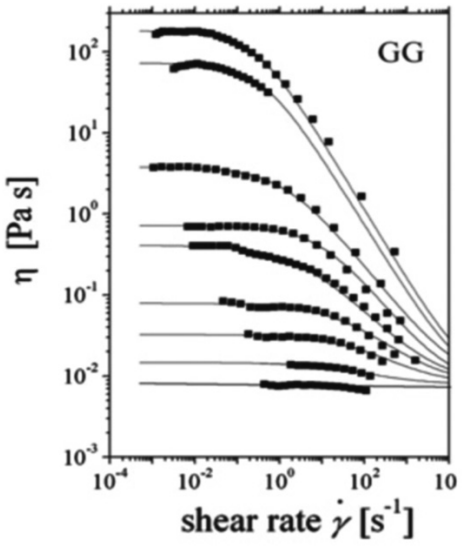

Fig. 54 Shear rate dependence of the viscosity of guar gum aqueous solutions at different concentrations (40 °C). The full lines represent the calculated values according to the Cross equation[214].

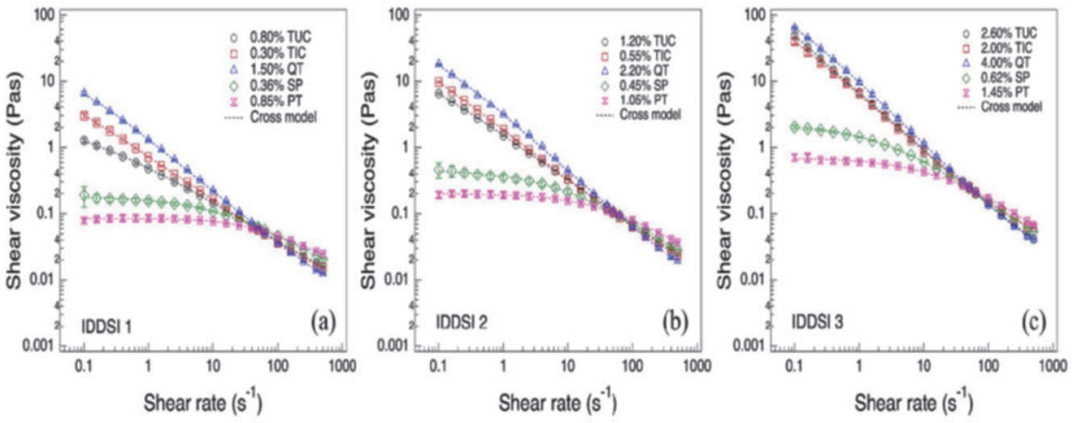

Fig. 55 Flow curves of different thickened liquids showing shear viscosity as a function of shear rate for different levels of liquid consistency (a) IDDSI level 1, (b) IDDSI level 2 and (c) IDDSI level 3. For each IDDSI, the concentration of each liquid was selected to have similar viscosity at shear rate 50 s^{-1}. TUC (Xanthan gum (33 %), maltodextrin (66.4 %), KCl (0.6 %)), TIC (Xanthan gum, maltodextrin, ascorbic acid), QT (Xanthan gum, maltodextrin, dextrose, $Ca_3(PO_4)_2$), SP (Guar gum (100 %)) PT (Tara gum, maltodextrin, $CaCO_3$)[215].

in the situation of wine tasting. In such a situation, the fluid may stay quiescently before being swallowed, and thus *Th* would be perceived at low strains.

As mentioned above, the comparison of the complex viscosity and steady shear viscosity is sometimes useful to understand the structural difference of fluids. When the complex viscosity $\eta^* = G^*/i\omega$ as a function of angular frequency ω, and the steady shear viscosity η as a function of shear rate $d\gamma/dt$ are plotted, the so-called Cox-Merz plot, both viscosities have been found to coincide for many flexible polysaccharide solutions. When the complex viscosity and the steady shear viscosity do not coincide, it may mean that the microstructure at the relaxed state is destroyed by shear force. Xanthan solutions don't obey the Cox-Merz rule because of its weak network structure while guar gum solutions have been shown to obey the Cox-Merz rule. However, other groups did not find that guar gum solution obeyed the Cox-Merz rule. Therefore, it is necessary to check carefully the validity of this rule[209].

The relation between the perceived thickness *Th* and the instrumentally measured viscosity η_N of Newtonian fluids (corn syrups) has been studied using 60 normal volunteer participants, aged 21-84 years[217]. Smith *et al.*[217] found the power law exponent β in $Th \sim \eta_N^{\beta}$ *ca.* 0.33 for both oral perception and oropharyngeal perception. This value agreed well with previously obtained by Christensen and Casper[218] irrespective of sensory modalities: 0.34 for oral, 0.39 for visual, and 0.35 for tactile judgments. Smith *et al.*[217] found the decrease in the exponent with the age as expected and reported, consistent, for example, with the decrease in the tongue pressure[6].

Recently, another method of analysis using a model that *Th* was proportional to the shear stress σ perceived at the surface of the tongue when the fluid was squeezed between the tongue and the palate during the transportation process of the ingested fluid to the posterior part of the mouth[219]. Deblais *et al.*[219] analysed the flow of power law fluids between two rigid plates representing the tongue surface and the hard palate assuming that fluid is a power law fluid with the consistency parameter κ and the power law index *n*. When the bottom plate (tongue) moves at a speed *V* relative to the top (palate) to deform the trapped liquid, the shear stress σ is given by

$$\sigma = \kappa V^n h_0^{-n} \left(1 + \frac{(n+1) F_N h_0^{n+1} V^{1-n}}{2\pi n \kappa R^4} t\right)^{\frac{n}{n+1}}, \qquad (3)$$

where h_0 is the initial gap between the tongue and the upper part of the oral cavity, *R* is the radius covered by the liquid product on the tongue, F_N is the lingual force, and *t* is the characteristic time needed for assessment (*i.e.* the residence time for the liquid product during the sensory test). Deblais *et al.*[219] examined whether the relation between the thickness *Th* and stress σ followed the power law proposed by Stevens; $Th = A\,\sigma^b$ or the logarithmic dependence of Weber-Fechner; $Th = A\,\log(\sigma)$. Fluids used were bouillon soup with various concentrations with negligible yield stress. Including previous data[220], Deblais *et al.*[219] found that the relation between *Th* and σ was described well by Weber-Fechner for these power law fluids (Fig. 56).

All these authors[219, 220] stressed that further study is needed to take into account the presence of the yield stress when the above analysis is extended to more complex fluids.

In the study of the effect of bolus rheology on swallowing, most rheological measurements have been done using torque detection rheometer with a narrow gap geometry of parallel plate, cone plate and coaxial cylinder. These measurements have been useful to characterise quantitatively the rheological properties, but not applicable for inhomogeneous foods such as porridge, fruit jellies or jams containing fruit fragments when particle size exceeds 1mm. An ultrasonic spinning velocity (USV) profile method has been developed and applied to such inhomogeneous foods. Figure 57 shows a typical setup of USV[221, 222].

Since the fluid contacting the wall moves with the same velocity of the wall and the central point does not move, the velocity component $u_\theta = u_\xi r/\Delta y$ is given by $u_\theta\,(r = R,\, t) = U_{wall} \sin(2\pi ft)$ and $u_\theta\,(r = 0,\, t) = 0$, where the velocity of the wall U_{wall} is given by $U_{wall} = 2\,\pi f\, R\, \Theta$, Θ is the oscillation angle amplitude and *f* is the frequency. Rheological properties of three different jellies made from LMP (low methoxy pectin)

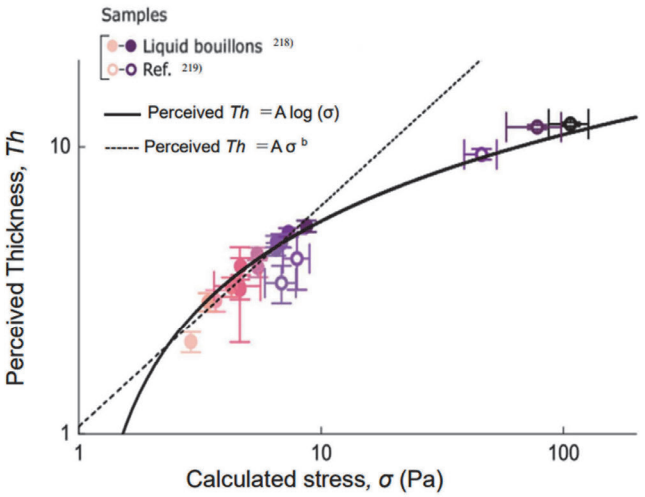

Fig. 56 Relation between subjective thickness *Th* and stress σ on the tongue as calculated[218, 219]. The black continuous line indicates a logarithmic dependence (Weber-Fechner's law), while the black dotted line shows a power law-dependence (Stevens' law)[219].

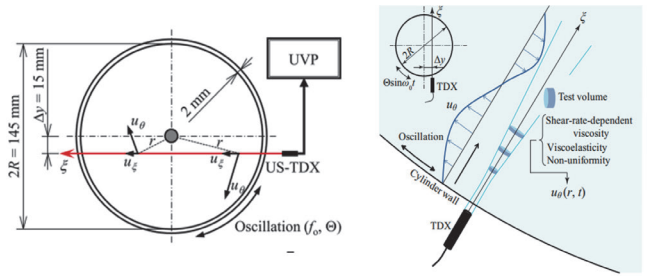

Fig. 57 Concept of ultrasonic spinning rheometry (a) top view of the rotating cylinder. US-TDX, ultrasonic transducer. The ultrasonic velocity profiling (UVP) measures the velocity component u_ξ parallel to the ultrasonic propagation line ξ at each measurement point on the line. Azimuthal velocity component $u_\theta = u_\xi r/\Delta y$ is $u_\theta\,(r = R,\, t) = U_{\mathrm{wall}} \sin(2\pi ft)$, $u_\theta\,(r = 0,\, t) = 0$, $U_{\mathrm{wall}} = 2\pi^2 fR\Theta/180$[222, 223].

source mixed with milk at different mixing ratios 1) 2:1; 2) 1:1; 3) 1:2 (Fig. 58) were observed by both conventional rheometer detecting torque and USV.

In the Fig. 59 (a)-(c), the shear stress first showed an overshoot as has been observed widely in simple yield stress fluids[224]. When the stress reached a certain value, the strain increased without increasing stress showing a plateau, which may be ascribed to slippage. Due to the presence of viscous component, a phase lag occurs between the stress and strain. Assuming a Maxwell element (a series combination of a spring and a dashpot), and performing Fourier transform, Yoshida *et al.*[223] obtained the flow curves, shear stress - shear rate curves, at each instant as shown in Fig. 60.

Although the gradient of the double logarithmic plot of shear stress-shear rate at terminal stage (tf_0 = 1800–1900) was lowest for milk: source = 1:2 mix (Fig. 60(d)), this sample showed a higher stress at earlier stage (Fig. 60(c)). The larger shear stress observed locally at the lowest shear rates in the earlier period for milk: source = 2:1 mix (Fig. 60(a)) was found similar to typical flow curves observed in shear banding fluids[225]. The decrease in the shear stress at earlier stage (tf_0 = 0–4) for milk: source = 1:1 mix (Fig. 60b) showed the structure break down. These transient flow curves were not reported by conventional rheometers and could be ob-

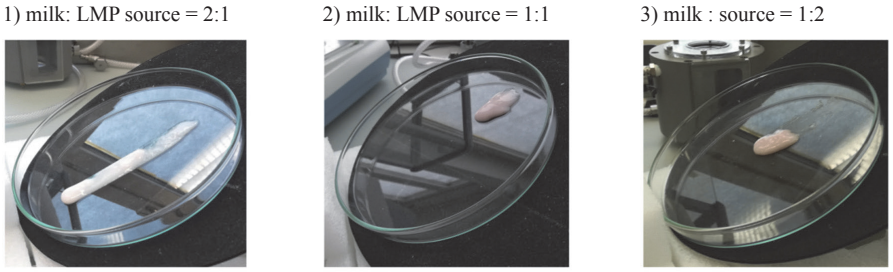

Fig. 58 Photographs of three different jellies made from LMP with milk[223].

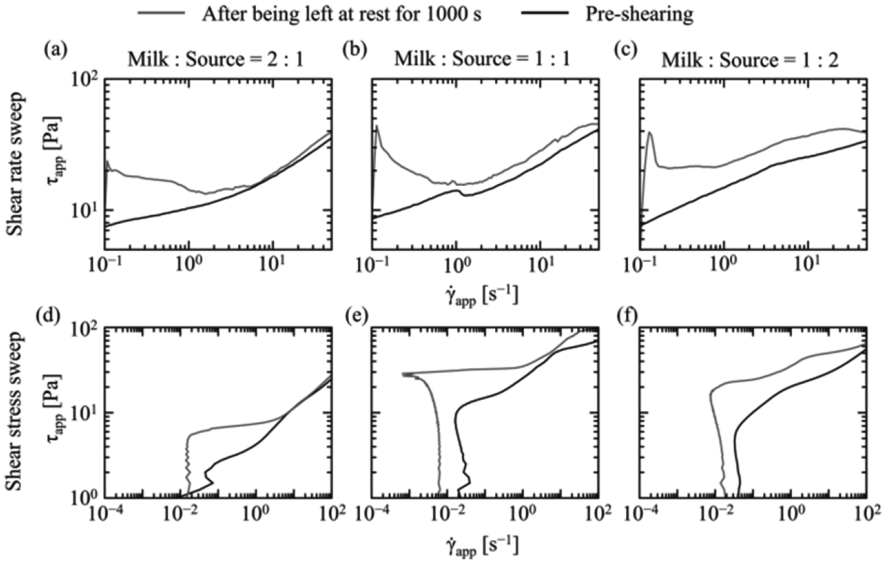

Fig. 59 Rheological evaluations by the steady rotational tests with a parallel plate rheometer for three different jellies made from LMP with milk shown in Fig. 58: (a)-(c) shear strain rate controlled measurements and (d)-(f) shear stress controlled measurements; gray and black curves represent flow curves obtained after being left at rest for 1000 s and immediately after the preshearing. Note that although the ordinate is the shear stress in (d)-(f), it is the independent variable, and the abscissa shear rate is dependent variable[223].

served by USP.

In addition to these inhomogeneous food materials, rheological properties of curry paste[226] and rice porridge[227] have been reported by the same group. This emerging method USP is promising, and, needs verification and validation with sensory evaluation to assess how the measurement can be useful and effective for describing ease of swallowing.

8. YIELD STRESS IN THE SWALLOWING

Steady shear viscosities of xanthan and LBG solutions with different concentrations were compared[67]. The yield stress was determined as the maximum in the plot of the elastic stress (= storage modulus × strain) vs. strain (Fig. 61). While xanthan gum solutions showed such a maximum, LBG solution did not show such a maximum because the former is a so-called weak gel or structured liquid while the latter is a common normal polymer solution without such a structure. A similar tendency was reported recently for xanthan, carboxymethylated curdlan (CMCD) and konjac glucomannan (KGM); when the elastic stress plotted against strain, xanthan and CMCD showed a maximum while KGM did not show such a peak[228].

The yield stress and yield strain for xanthan gum

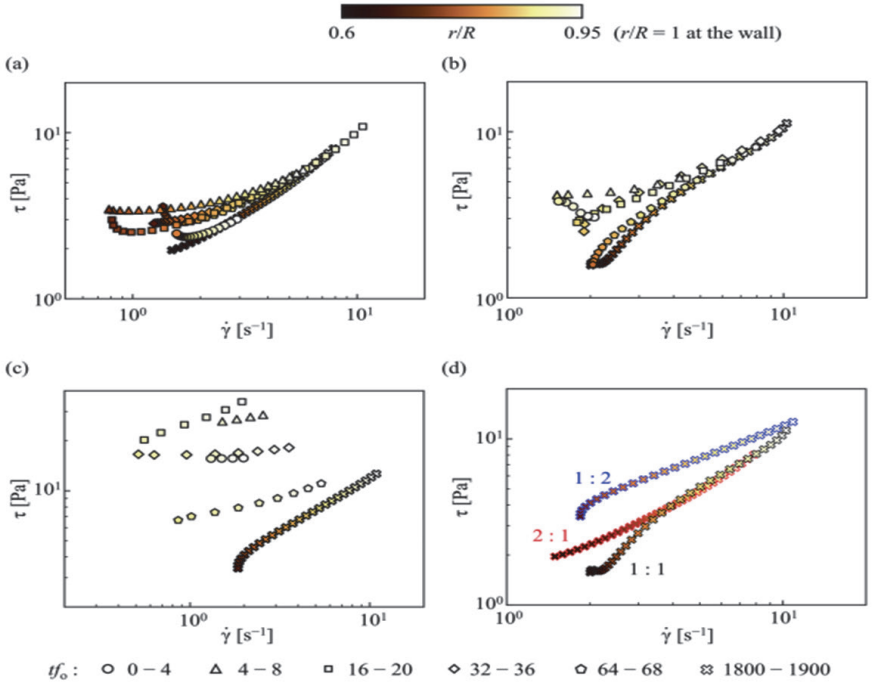

Fig. 60 Flow curves at different oscillating cycles; (a) milk: source = 2:1 mix, (b) milk: source = 1:1 mix, and (c) milk: source = 1:2 mix, and (d) terminal flow curves at tf_0 = 1800–1900 in each test material, with the oscillation frequency, amplitude, temperature, and the maximum angular velocity, f_0 = 1.0 Hz, $\Theta = \pi/3$, T_0 = 15 °C, and U_{wall} = 477 mm/s, respectively[223].

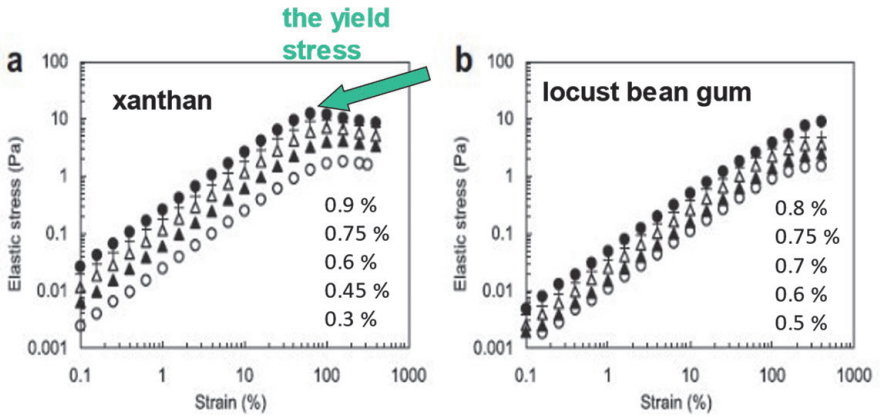

Fig. 61 Elastic stress (storage modulus multiplied by strain) of xanthan gum and locust bean gum solutions at 20 °C plotted as function of strain. The yield stress and strain were estimated from the maximum point in the curve (Nakauma *et al.* [67]).

solutions with different concentrations are shown in Table IX. While the yield stress increased, the yield strain decreased with increasing concentration of xanthan gum.

Yield stress is sometimes not well understood. Yield stress is a minimum stress above which the material begins to flow, and can be measured by extrapolating the shear rate to zero in the plot of stress vs shear rate[209, 229]. The yield stress determined by this procedure is called dynamic yield stress. When the shear rate is increased from zero, the yield stress which is given by the intercept in the plot of stress vs shear rate is called static yield stress. For thixotropic materials, some structure is formed during the time when the stress is kept zero, and thus the static yield stress is found larger than the dynamic yield stress. Barnes[230] was skeptical about the existence of the yield stress saying that everything flows. He showed that there is a viscosity plateau for four fluids, tooth paste, Carbopol (CMC solutions), tomato puree, and mayonnaise. According to him, the yield stress marks a transition between two fluid states that are not fundamentally different - but with very different viscosities (Fig. 62).

This problem was revisited using the same sample carbopol[231]. It was found that when the apparent viscosity is measured by decreasing the shear stress, the viscosity steeply increased at around the stress of 27 Pa, and diverged at 27 Pa, indicating that the sample didn't flow (Fig. 63A). This stress 27 Pa was defined as the yield stress. It was also found that the viscosity showed a Newtonian plateau below the yield stress (Fig. 63B). This means that the fluid flowed below the yield stress, which is contradictory to the definition of the yield stress.

Then, Mϕller, Fall and Bonn[231] tried to show that the plateau below the yield stress is induced by the measurement for non-steady shear flow. They measured the viscosity of four substances: A) 0.2 % Carbopol, B) hair gel, C) foam, D) emulsion (Fig. 64), and found that there was a plateau below a certain value of the stress as shown by Barnes[230]. However, they found also that this plateau was an apparent value observed at a non-equilibrium state. When the plateau value was plotted against the time, the viscosity value was found to increase according to the power law

$$\eta \sim t^{n} \tag{4}$$

The apparent viscosity of 0.2 % carbopol as a function of time for different stress values was plotted in Fig. 65. Above the stress 27 Pa, the apparent viscosity quickly

Table IX Yield stress and strain of xanthan gum solutions. Data are presented as means ± SD of triplicates. Values with different letters (a-e) are significantly different ($p < 0.05$)[67].

Concentration (%)	Yield stress (mPa)	Yield strain (%)
0.3	1524 ± 142 a	120.6 ± 1.5 a
0.45	4035 ± 155 b	97.0 ± 4.0 b
0.6	6917 ± 372 c	88.1 ± 6.9 b
0.75	8518 ± 387 d	65.3 ± 8.5 c
0.9	10,043 ± 472 e	56.3 ± 5.0 c

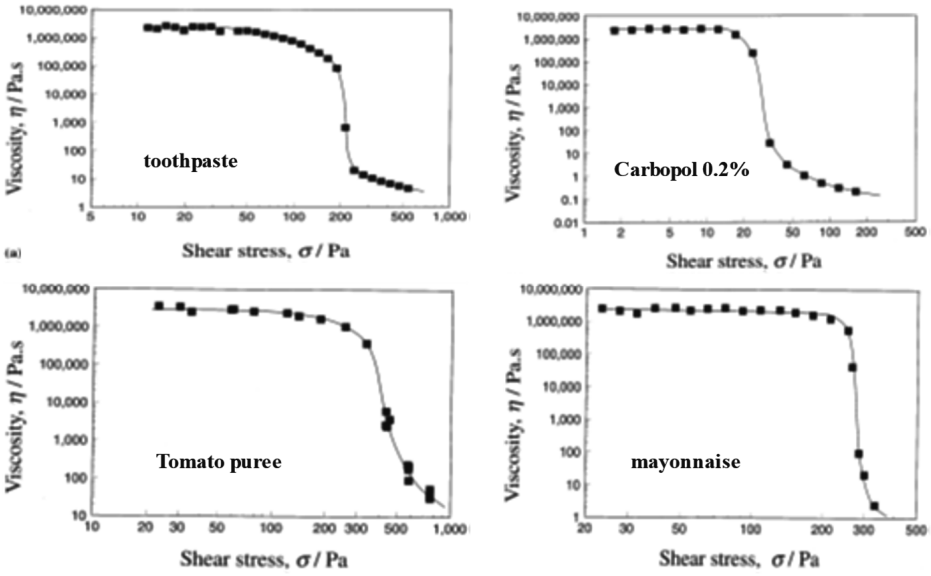

Fig. 62 The viscosity as a function of shear stress for four common fluids, toothpaste, 0.2 % Carbopol (carboxymehyl cellulose solution), tomato puree, mayonnaise[230].

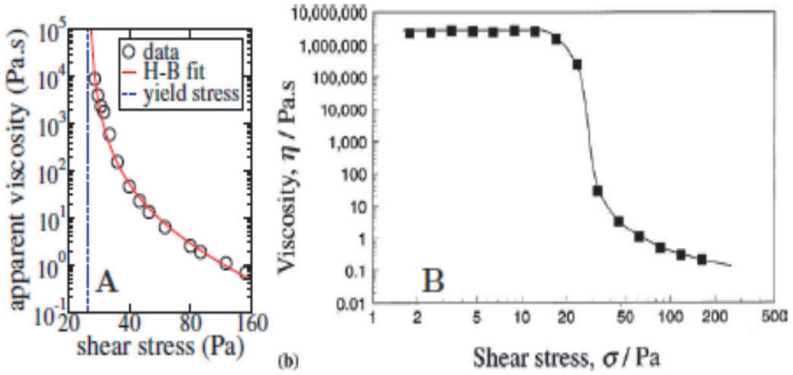

Fig. 63 A) The Herschel-Bulkley model provides a good fit to the viscosity of a carbopol sample (0.2 %mass at pH = 7) as the stress σ is lowered towards the yield stress. B) Measurements on an identical carbopol sample apparently demonstrate the existence of a Newtonian limit below the "yield stress" (Barnes, 1999). This figure is representative of the figures claimed to demonstrate that yield stress materials flow below the yield stress[231].

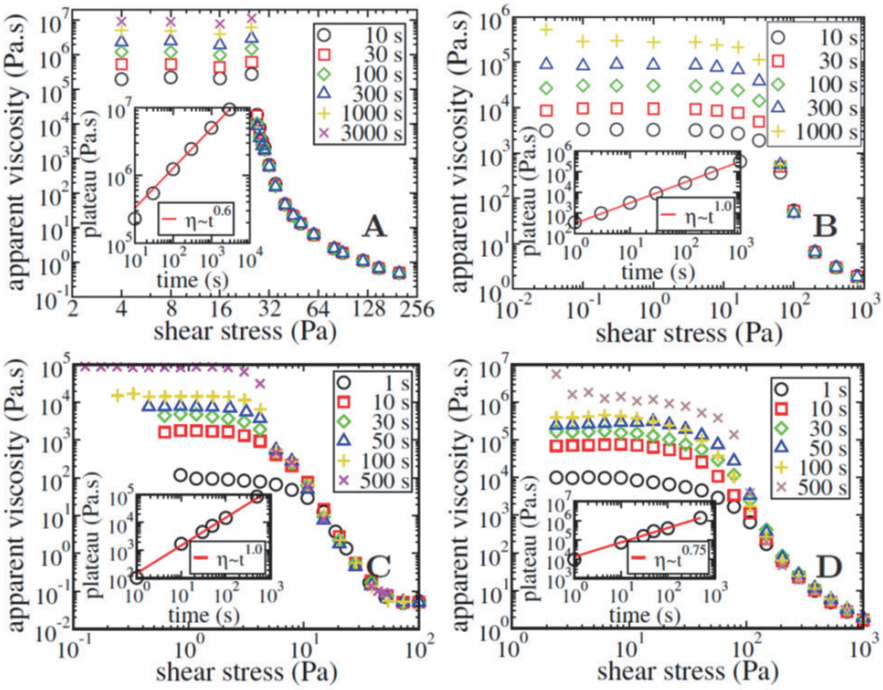

Fig. 64 Viscosity as a function of shear stress for four samples: A) The 0.2 % carbopol sample. B) The hair gel. C) The foam. D) The emulsion. The resulting curves resemble those in Fig. 62, but the values of the plateaux increase with measurement time. The insets show that the plateaux increase as power laws with time with exponents in the range 0.6-1.0[231].

reaches the steady value and then it stays constant up to ~ 10^3 s, while below the stress 25 Pa, the apparent viscosity continues to increase even at 10^4 s. Therefore, above the stress 27 Pa, the material flows at a constant viscosity which is a decreasing function of the stress, while the apparent viscosity continues to increase with time as $\eta \sim t^{0.6}$ as shown by the dashed straight line, indicating that the system behaves almost as a solid having a very large viscosity within the experimentally accessible observation time. Thus, this stress 27 Pa can be defined as a yield stress.

Reiner[232] pointed out that Prophetess Deborah who, in the Book of Judges, proclaimed "The mountains flowed before the lord", knew two things: First, that the mountains flow, as everything flows. But, secondly, that they flowed before the Lord, and not before man, for the simple reason that man in his short lifetime cannot see them flowing, while the time of observation of God is *infinite*. We may therefore well define a nondimensional number the Deborah number D = time of relaxation/time of observation. Therefore, we had better leave "Heraclitus" *παντα ρει* as **a special case for infinite time of observation**, or infinitely small time of relaxation. The greater the Deborah number, the more solid the

material; the smaller the Deborah number, the more fluid it is"[232]. This should be taken into account when we determine the yield stress.

Figure 66 shows the creep compliance of the same data. At and below the stress 25 Pa the deformation was zero indicating the solid behavior below this critical stress (yield stress), while the compliance increases with increasing time with the slope 1 indicating the fluid behavior at and above the stress 27 Pa. The yield stress is a function of the amount of structure breakdown during flow[233, 234].

To generalize the definition of yield stress to materials which are thixotropic, it is necessary to distinguish the static yield stress and the dynamic yield stress. The thixotropy is defined as the decrease in the viscosity at a constant shear rate with the lapse of time. It is different from shear thinning behavior which is defined as the decreasing of the viscosity when the shear rate is increased. All the shear thinning liquid show a thixotropic behavior since it takes a time to recover the initial microstructure even if it is short[209, 233, 235-237]. It is necessary to note that the dynamic yield stress corresponds to an infinite failure-time and the static yield stress to an immediate failure. For non-thixotropic yield stress materials, the dynamic yield stress and static yield stress coincide. For thixotropic materials, some interconnected structure in polymer chains or colloidal particles is existing before the shearing, and the minimum shear stress necessary to make flow, called a static yield stress, is known to be larger than the value obtained from an equilibrium stress-strain rate curve, which is a dynamic yield stress.

The delayed fracture phenomenon was studied in relation with yield stress for a fish protein, extracted from cods and haddocks, soft gels[238]. The storage modulus (1 Hz) for fish protein gels heated at different temperatures (30–70 °C) as a function of strain showed a maximum at a fracture strain. The stress at fracture obtained in this way is equal to the dynamic yield stress σ_d above which the systems flow immediately during constant application of stress[239]. The time-to-failure t_f as a function of the scaled stress σ/G_0 is plotted in Fig. 67[238]. As suggested by previous papers[240, 241], the time-to-fracture of colloidal gels scales differently over two limiting regimes of stress. In the low-stress regime where bond fracture is followed by reformation, the fracture of entire colloidal strands is strongly delayed, while in the high-stress regime a strand breaks once all the bonds forming it have broken with negligible bond reformation. This leads to an exponential dependence of t_f on the stress with two distinct regimes identified[240, 241]:

$$t_f = \frac{1}{C\sigma n^2 k_A}\left(\frac{k_A}{k_D}\right)^n e^{-nc\sigma} \text{ (dominant bond reformation)} \quad (5)$$

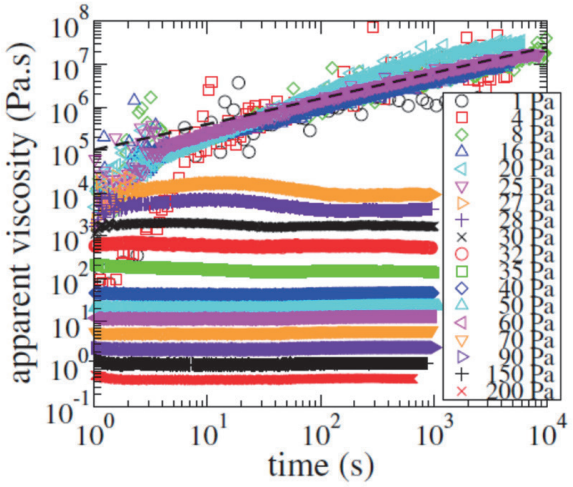

Fig. 65 The apparent viscosity of 0.2 % carbopol as a function of time for different stress values[231].

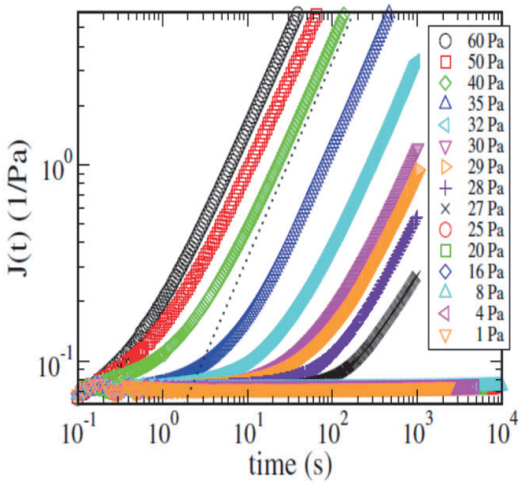

Fig. 66 Creep compliance of 0.2 % carbopol as a function of time for different stress values[231].

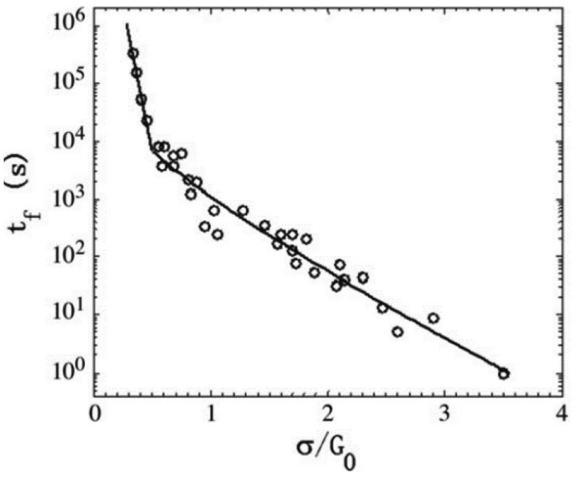

Fig. 67 Time to failure t_f as a function of the scaled applied stress σ/G_0 for fish protein soft gels. The solid lines are fits to Eqs. (5) and (6). G_0 is the high-frequency plateau shear modulus[238].

$$t_f = \frac{\Sigma_{j=1}^{n} 1/j}{C\sigma k_D} e^{-c\sigma} \text{ (negligible bond reformation)} \quad (6)$$

where k_A is the bond reformation constant, k_D is the bond dissociation constant, n is the number of bonds per strand, and C is a constant reflecting the fracture energy of the strands[240, 241]. From the curve fitting, the bond dissociation constant, $k_D = 1.2 \times 10^{-4}$ s^{-1}, bond reformation constant $k_A = 7.4 \times 10^{-4}$ s^{-1}, and the average number of bonds per strand $n = 9$ were obtained. Taking into account $Sn = (\Sigma_1^n 1/j) = \varepsilon + \ln n$, where $\varepsilon = 0.5772$ (Euler's constant), and the crossover of the stress occurs at $\ln(k_A/k_D)/C$, the crossover stress was found to be $\sigma_{cross} = \ln(k_A/k_D)/C = 1.14/C$.

However, as Sprakel *et al.*[240] explained, the two equations are only limiting laws, which only hold far away from the crossover regime. At stresses close to the crossover, both types of fracture can initiate the macroscopic failure of the gel. Thus, Sprakel *et al.*[240] reached at $\sigma_{cross} = 1.82/C$ from physical arguments. Finally, numerical fitting led to the result $\sigma_{cross} = 1.82/C = 0.8\ G_0$.

In Fig. 67, the crossover is found at $\sigma_{cross} = 0.55\ G_0 < 0.8\ G_0$. An experimental finding that the experimentally observed critical (crossover) stress is slightly lower than theoretically predicted value, is in line with previous reports for 8 % carbon black gels where an experimental crossover stress 20 Pa was slightly smaller than a computed critical stress 24 Pa[240, 241]. Although the theoretical calculation was only an order-of-magnitude estimate to derive the crossover stress $\sigma_{cross} = \ln(k_A/k_D)/C$ separating the two stress regimes, this quantitative agreement might be fortuitous but the approximation was also grabbing an essential point.

Yield stress of food and related materials has further been studied recently[237, 242]. Lissajous presentation of stress-strain and stress-strain rate curves has been widely used because it is useful for geometrical interpretation[209]. The general geometric average requires the calculation of the arithmetic mean of the stress and the strain rate in a cycle of oscillatory shear as shown in an example for 80 % polydimethyl-siloxane (PDMS) emulsion (Fig. 68)[242].

The endpoints of the geometric average curves ($\sigma_{max} \sim \bar{\gamma}_{max}$, $\bar{\sigma}_{max} \sim \gamma_{max}$, $\sigma_{max} \sim \bar{\dot{\gamma}}_{max}$, $\bar{\sigma}_{max} \sim \dot{\gamma}_{max}$) together with $\sigma_{max} \sim \gamma_{max}$ for 80 % PDMS emulsion with different stress amplitudes are shown in Fig. 69(a). As can be seen, both curves $\sigma_{max} \sim \bar{\gamma}_{max}$ and $\bar{\sigma}_{max} \sim \gamma_{max}$ superpose at low stress level with a slope 1, indicating the linear stress-strain relation, that is, ideal linear elastic behaviour. Further increase in stress made the stress-strain relation deviate from the linearity and the bifurcation appeared. The bifurcation points for the $\sigma_{max} \sim \bar{\gamma}_{max}$ curve and $\bar{\sigma}_{max} \sim \gamma_{max}$curve coincided with that for $\sigma_{max} \sim \gamma_{max}$. The bifurcation strain and stress were defined as start yield strain $\gamma_{y,start}$ and start yield stress $\sigma_{y,start}$, respectively. Actually, $\sigma_{y,start}$ (or $\gamma_{y,start}$) can be regarded as the maximum stress (or strain) to sustain solid-like behaviour, and the solid-liquid transition cannot happen below such stress (or strain). In the stress-strain rate relation, $\sigma_{max} \sim \bar{\dot{\gamma}}_{max}$ and $\bar{\sigma}_{max} \sim \dot{\gamma}_{max}$ curves are found to superpose at high stress level and bifurcate as stress decreases, and the $\sigma_{max} \sim \bar{\dot{\gamma}}_{max}$ curve bifurcated at the same point. The bifurcation stress and strain rate could be defined as end yield stress $\sigma_{y,end}$ and end yield strain rate $\dot{\gamma}_{y,end}$, respectively. $\sigma_{y,end}$ corresponds to the minimum stress above which complete solid-liquid transition happens in an oscillatory shear cycle. It is seen from Fig. 69 that $\sigma_{y,end}$ is larger than $\sigma_{y,start}$ for 80 % PDMS.

The stress-strain and the stress-strain rate curves observed in the shear stress ramp experiments are shown in Fig. 69(b). The stress-strain curves superposed at low stress

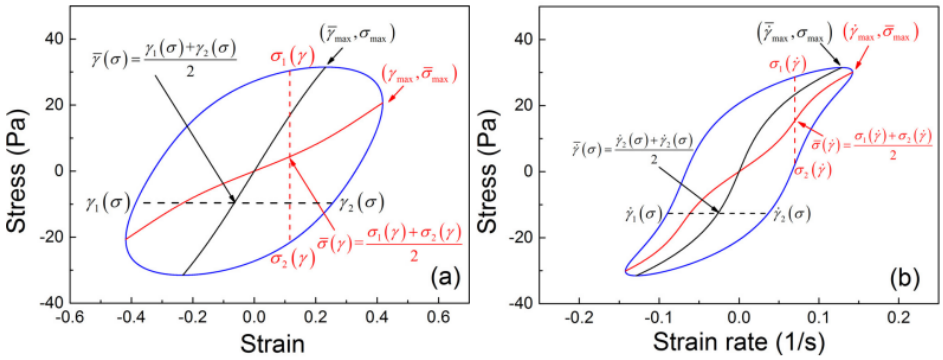

Fig. 68 Geometric average representation of Lissajous curves for 80 % PDMS emulsion at 0.005 Hz and stress amplitude 31.5 Pa. (a) Mean stress $\bar{\sigma}(\gamma)$ and strain $\bar{\gamma}(\sigma)$ are given by the middle point of broken line connecting $\sigma_1(\gamma)$ and $\sigma_2(\gamma)$, and $\gamma_1(\sigma)$ and $\gamma_2(\sigma)$, respectively. The endpoints ($\bar{\gamma}_{max}$, σ_{max}) and (γ_{max}, $\bar{\sigma}_{max}$) are indicated. (b) Mean stress $\bar{\sigma}(\dot{\gamma})$ and strain rate $\bar{\dot{\gamma}}(\sigma)$ are given by the middle point of broken line connecting $\sigma_1(\dot{\gamma})$ and $\sigma_2(\dot{\gamma})$, and $\dot{\gamma}_1(\sigma)$ and $\dot{\gamma}_2(\sigma)$, respectively. The endpoints ($\bar{\dot{\gamma}}_{max}$, σ_{max}) and ($\dot{\gamma}_{max}$, $\bar{\sigma}_{max}$) are indicated. γ_{max} and $\dot{\gamma}_{max}$ represent the amplitude of strain and strain rate, while σ_{max} represent the amplitude of stress, respectively[242].

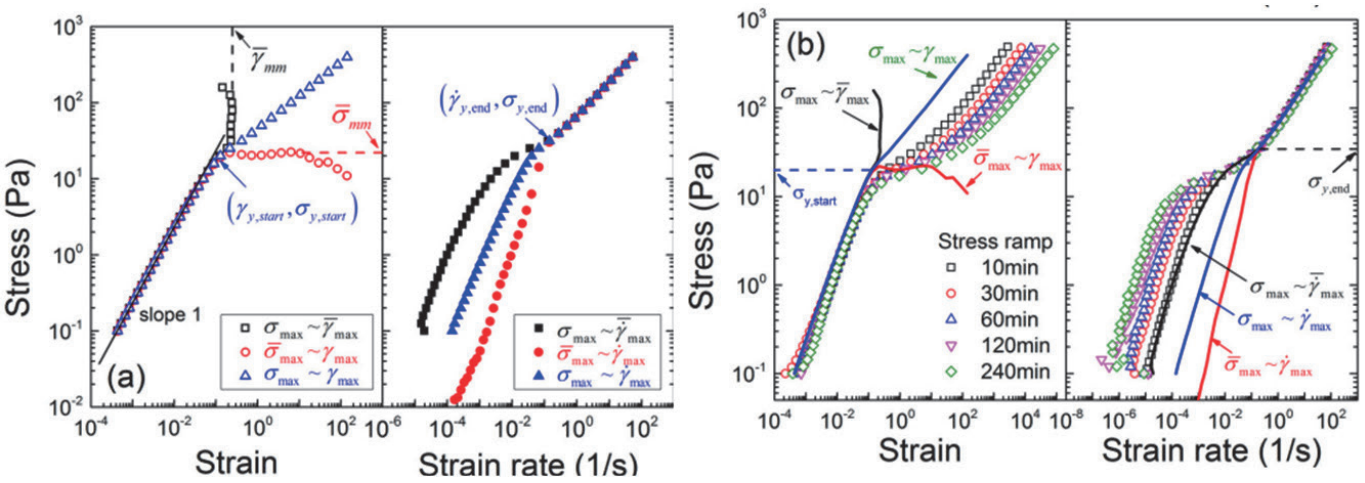

Fig. 69 Stress bifurcation between endpoint curves of 80 % PDMS observed in LAOS stress at 0.05 Hz where $\overline{\gamma}_{mm}$ and $\overline{\sigma}_{mm}$ represent the maximum in mean strain and the maximum in mean stress, respectively (a), and comparisons with the results of shear stress ramp under different ramp times; the endpoint curves in LAOS exhibit instinct characteristics, *i.e.*, they bifurcate with increasing stress at $\sigma_{y,start}$ in stress-strain relation, and with decreasing at $\sigma_{y,end}$ in stress-strain rate relation (b)[242].

level indicating the linear elastic solid behaviour, and the stress-strain rate curves superposed at high stress level indicating the liquid-like behaviour. The boundary region connecting the solid-like region and the liquid-like region was identified as the yield transition, which was more apparent as the ramp time was longer.

The determination of the yield stress of thixotropic materials is complex. The yield stress for solutions and emulsions of xanthan, carboxymethylated curdlan (CMCD), and KGM was examined[237]. Emulsions were prepared by adding certain amounts of pea protein (4 wt%), soybean oil (4 wt%), and maltodextrin (12 wt%) into 0.5 wt% polysaccharide solutions. The thixotropic behaviour has been studied by examining the hysteresis loop, up-curve and down-curve of stress -strain rate, as shown in Fig. 70.

The area enclosed by the hysteresis loop represents the extent of the thixotropic behavior, and was evaluated as 51 Pa s^{-1} for XG emulsion and 770 Pa s^{-1} for CMCD emulsion. The greater hysteresis area for CMCD emulsion than that for xanthan emulsion was attributed to the hydrogen bonding associations among CMCD chains with triple helical conformation leading to the formation of a stronger interaction network and denser compact aggregation inside the emulsion system[237].

In addition to the hysteresis loop method, when the sample is subjected to the suddenly stepping up or down the shear rate, the subsequent viscosity transients reflecting the changes in microstructure has been studied to understand the thixotropic nature[233, 236, 243-246]. Recently, Li *et al.*[247] used the three interval thixotropy tests in the study of thixotropic nature of xanthan, CMCD and KGM. The increase in G' at the rest intervals for the CMCD and XG solutions was attributed to the ability of the structural regeneration, while no resistance in recovery of G' of KGM solutions was found. Judging from the greater extent of the thixotropy, the structure rebuilding/rejuvenation of CMCD emulsions after shearing would need

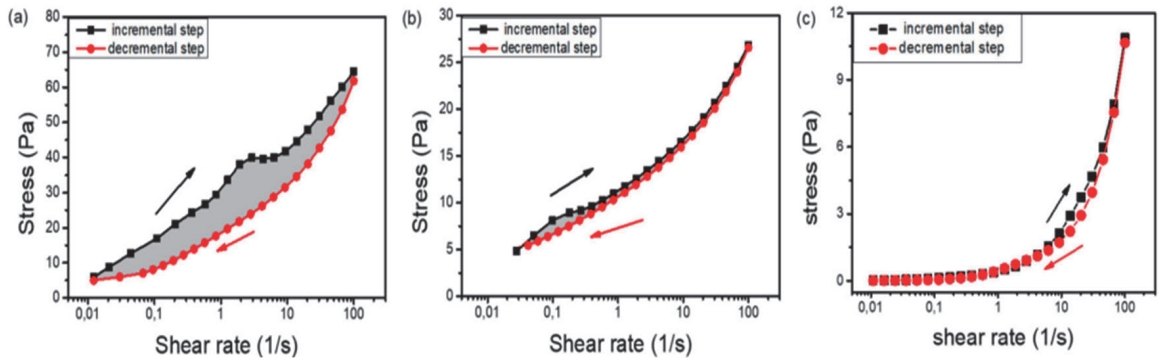

Fig. 70 The thixotropic properties of three polysaccharide emulsions: (a) CMCD, (b) xanthan, and (c) KGM emulsions at a polysaccharide concentration of 0.5 wt%. The up-curve with upward arrow and the down-curve with downward arrow show the shear rate increasing and decreasing process, respectively. The gray enclosed area by the up-curve and the down-curve indicates the hysteresis loop for CMCD and XG emulsions. The hysteresis area was 770 Pa s^{-1} for CMCD, 51 Pa s^{-1} for XG emulsion, and negligibly small for KGM[237]. Note that (a) and (b) in Fig. 70 were wrongly represented in Wei *et al.*[237].

a longer time to complete. During and after the oral processing, the thixotropic nature of the decrease in the viscosity with the lapse of time will be beneficial for bolus transport in the oropharyngeal and gastrointestinal organs. Li *et al.*[247] pointed out the necessity of microstructural study underlying the thixotropic behavior, and how this should be taken into account in the food design for dysphagia patients is a future problem in relation with physiological / anatomical / food processing / preservation consideration.

Stress bifurcation between endpoint curves of 0.5 % xanthan observed in LAOS at 0.5 Hz is shown in Fig. 71.

The yield stress of CMCD and xanthan solutions and emulsions by other methods were determined, and the values are shown in Fig. 72[237].

As shown in Fig. 72, the yield stress values are different depending on the measurement method. The difference is significant especially for thixotropic materials; CMCD emulsions showed a strong thixotropic nature, large hysteresis area as shown in Fig. 70.

When swallowing, the soft palate is elevated to seal off the nasopharynx, preventing postnasal bolus leaking as shown in Fig. 7(b)[75] (Part 1 of this review). If the food bolus showed as a fluid like viscoelastic body, its security risk will be very small, because it can pass through the pharynx in a very short time without causing suffocation, unless its viscosity exceeds a certain limit.

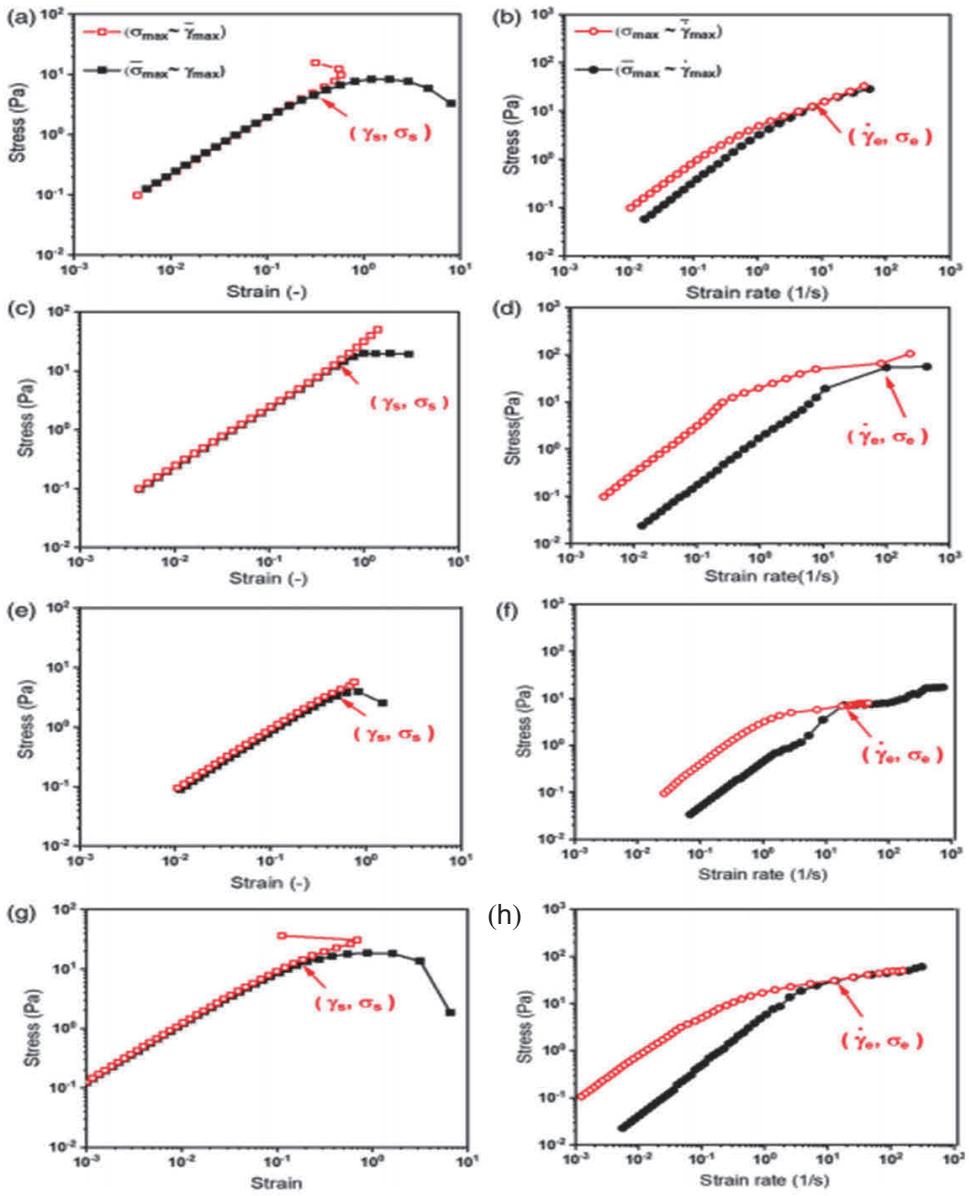

Fig. 71 Stress bifurcation between end point curves of 0.5 wt% CMCD and xanthan solutions, and thickened emulsions from LAOS at 0.5 Hz: (a) stress vs strain and (b) stress vs shear rate for CMCD solutions; (c) stress vs strain and (d) stress vs shear rate for CMCD emulsions; (e) stress vs strain and (f) stress vs shear rate for xanthan solutions; and (g) stress vs strain and (h) stress vs shear rate for xanthan emulsions. Bifurcation occurs with increasing stress at $\sigma_{y,start}$ in stress-strain relation (a), (c), (e), and (g), and with decreasing at $\sigma_{y,end}$ in stress-strain rate relation (b), (d), (f), and (h)[237].

Whether the food bolus exhibits stress relaxation and elastic recovery would mainly depend on the nature of the food itself, such as beverage or gel candy. However, most of the time, food bolus is flowable regardless of whether the food bolus exhibits stress relaxation and elastic recovery, because even gel candy can be chewed and destroyed, and then mixed with saliva to form a flowable body. Therefore, the impact of stress relaxation and elastic recovery of food bolus on swallowing safety has not received much attention. Only recently, some new light was shed upon this problem[228].

Creep measurements for these polysaccharide solutions and emulsions were performed to get more insight in relation with the rheological behaviour in the mouth[228]. During the time when the tongue transfers the bolus to the posterior region in the mouth, deformation and/or recovery of bolus under certain stress should be an important parameter in safe swallowing. The deformation recovery properties of solutions and emulsions are shown and compared in Fig. 73.

While γ_e originates from the elastic restoring force after the removal of the external force, γ_v represents the strain related with a dissipated energy and thus not recoverable. While instantaneous compliance (intercept of deformation axis at $t = 0$) for KGM and xanthan was zero and very small for KGM and xanthan, CMCD solution and emulsion showed a larger value indicating the elastic nature. While CMCD solution showed a small deformation ($\gamma = 0.25$ %) and the ratio $\gamma_e/\gamma_v = 1.27$, $\gamma = 0.03$ % and $\gamma_e/\gamma_v = 50$ were observed for CMCD emulsion, indicating the resistance to the structural deformation by storing energy inside the internal association and a high recovering elastic ability, and this was found more conspicuous in the emulsion. Xanthan showed similar tendency. A small deformation ($\gamma = 3$ %, $\gamma_e/\gamma_v = 0.11$ for solution and $\gamma = 0.23$ %, $\gamma_e/\gamma_v = 0.21$ for emulsion), showing the existence of certain network associations although weaker than

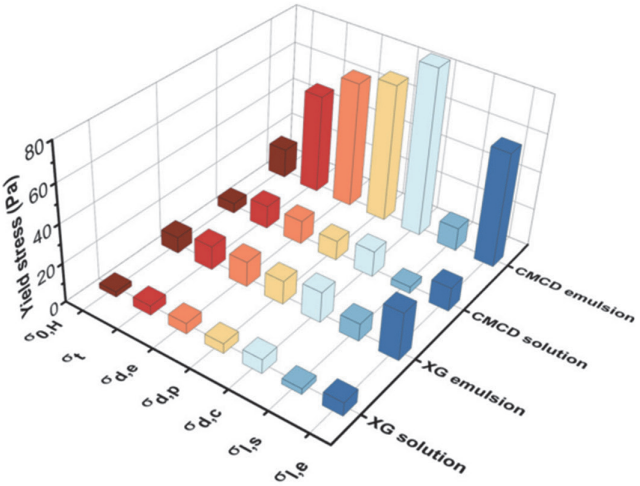

Fig. 72 Yield stress values determined by different measurement methods for 0.5 % CMCD and xanthan in solutions and thickened emulsions: $\sigma_{0,H}$, the value calculated from the Herschel-Bulkley model; σ_t, the end value of yield stress determined by the transient shear rate ramp method; $\sigma_{d,e}$, the yield stress determined by the maximum in the elastic stress curve; $\sigma_{d,p}$, the yield stress determined by the intersection of two power-law extrapolations at low and high-stress ranges in G' vs stress amplitude; $\sigma_{d,c}$, the yield stress determined by the crossover point of G' and G''; $\sigma_{l,s} = \sigma_{y,start}$, the start value of yield stress determined by LAOS curves; and $\sigma_{l,e} = \sigma_{y,end}$, the end value of yield stress determined by LAOS curve[237].

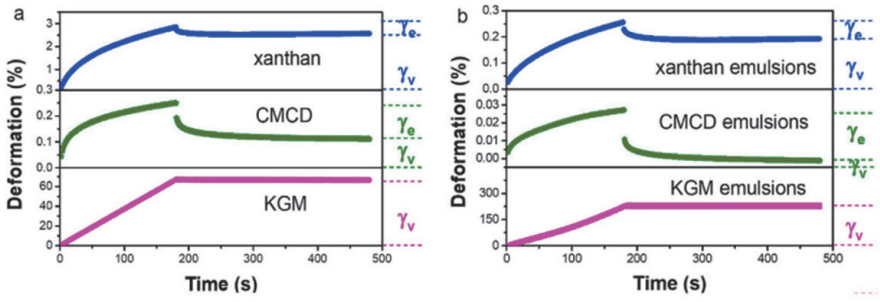

Fig. 73 Creep and creep recovery of polysaccharide solutions (a) and thickened emulsions (b) at a polysaccharide concentration of 0.5 %. A stimulus of a constant stress 0.5 Pa was imposed at the time $t = 0$ until $t = 180$ s, and the response strain was measured for 300 s The γ_e and γ_v represent the elastically recovered strain and viscous strain, respectively[228].

CMCD. However, the KGM solution shows an almost only viscous deformation with a quite large γ value of 66 % and a γ_e/γ_v value of almost zero. The finding that CMCD emulsion ($\gamma_e/\gamma_v = 50$) showed a higher elastic recovery ability than xanthan emulsion ($\gamma_e/\gamma_v = 0.21$) and KGM emulsion ($\gamma_e/\gamma_v \sim 0$) was consistent with its higher yield stress (Fig. 70) and strong network in the emulsion.

REFERENCES (EXTRACTS)

6) Machida N, Tohara H, Hara K, Kumakura A, Wakasugi Y, Nakane A, Minakuchi S, *Geriatr Gerontol Int*, **17**, 295 (2017).
26) Clave P, de Kraa M, Arreola V, Girvent M, Farre R, Palomera E, Serra-Prat M, *Aliment Pharmacol Ther*, **24**, 1385 (2006).
38) Nishinari K, Fang Y, Rosenthal A, *J Texture Stud*, **50**, 369 (2019).
41) Brenner T, Hayakawa F, Ishihara S, Tanaka Y, Nakauma M, Kohyama K, Achayuthakan P, Funami T, Nishinari K, *J Texture Stud*, **45**, 30 (2014).
51) Prinz JF, Lucas PW, *Proc Biol Sci*, **264**, 1715 (1997).
66) Ishihara S, Nakauma M, Funami T, Odake S, Nishinari K, *Food Hydrocoll*, **25**, 1016 (2011).
67) Nakauma M, Ishihara S, Funami T, Nishinari K, *Food Hydrocoll*, **25**, 1165 (2011).
75) Matsuo K, Palmer JB, *Curr Opin Food Sci*, **9**, 1 (2016).
100) Chen J, Lolivret L, *Food Hydrocoll*, **25**, 325 (2011).
110) Hanson B, Jamshidi R, Redfearn A, Begley R, Steele CM, *Ann Biomed Eng*, **47**, 2296 (2019).
111) Vickers Z, Damodhar H, Grummer C, Mendenhall H, Banaszynski K, Hartel R, Hind J, Joyce A, Kaufman A, Robbins J, *Dysphagia*, **30**, 702 (2015).
125) Chen J, Khandelwal N, Liu Z, Funami T, *Arch Oral Biol*, **58**, 293 (2013).
141) Takahashi J, Nakazawa F, *J Texture Stud*, **23**, 139 (1992).
173) Wang X, Chen J, *Curr Opin Colloid Interface Sci*, **28**, 22 (2017).
174) Nishinari K, Zhang K, Yang N, Gao Z, Gamonpilas C, Turcanu M, Peyron M-A, Fang Y, Nitta Y, Yao X, Zhao M, Ishihara S, Nakauma M, Funami T, Kohyama K, Moritaka H, Yoshimura M, Takemasa M, Hori K, Matsuo K, Michiwaki Y, Zhang Y, Singh N, Meng AGS, *Nihon Reoroji Gakkaishi (J Soc Rheol Jpn)*, **51**, 219 (2023).
175) Hayakawa F, Kazami Y, Ishihara S, Nakao S, Nakauma M, Funami T, Nishinari K, Kohyama K, *Food Hydrocoll,* **38**, 95 (2014).
176) Tomczyńska-Mleko M, Brenner T, Nishinari K, Mleko S, Szwajgier D, Czernecki T, Wesolowska-Trojanowska M, *Food Sci Technol Res*, **20**, 607 (2014).
177) Tomczyńska-Mleko M, Brenner T, Nishinari K, Mleko S, Kramek A, *J Texture Stud*, **45**, 344 (2014).
178) Brenner T, Tomczynska-Mleko M, Mleko S, Nishinari K, *J Texture Stud*, **48**, 487 (2017).
179) Clark R, in "*Gums and Stabilisers for the food industry 11*", Williams PA, Phillips GO (Eds), 217 (2002), Royal Society of Chemistry, Cambridge.
180) Bayarri S, Rivas I, Costell E, Durán L, *Food Hydrocoll*, **15**, 67 (2001).
181) de Loubens C, Magnin A, Verin E, Doyennette M, Trelea IC, Souchon I, *J Theor Biol*, **267**, 300 (2010).
182) Mathieu V, de Loubens C, Thomas C, Panouille M, Magnin A, Souchon I, *J Biomech*, **72**, 144 (2018).
183) Ng GCF, Gray-Stuart EM, Morgenstern MP, Jones JR, Grigg NP, Bronlund JE, *J Texture Stud*, **48**, 294 (2017).
184) Ross AIV, Tyler P, Borgognone MG, Eriksen BM, *J Food Eng*, **263**, 123 (2019).
185) Ong JJ, Steele CM, Duizer LM, *Food Hydrocoll*, **84**, 173 (2018).
186) Buettner A, Beer A, Hannig C, Settles M, *Chem Senses*, **26**, 1211 (2001).
187) Hayashi T, Kaneko H, Nakamura Y, Ishida T, Takahashi H, Yamada Y, *Jpn J Dysphagia Rehabil*, **6**, 187 (2002).
188) Kohyama K, Sawada H, Nonaka M, Kobori C, Hayakawa F, Sasaki T, *Biosci Biotechnol Biochem*, **71**, 358 (2007).
189) Li Q, Hori K, Minagi Y, Ono T, Chen YJ, Kondo J, Fujiwara S, Tamine K, Hayashi H, Inoue M, Maeda Y, *PLoS One*, **8**, e70850 (2013).
190) Funami T, Ishihara S, Nakauma M, Kohyama K, Nishinari K, *Food Hydrocoll*, **26**, 412 (2012).
191) Funami T, Matsuyama S, Ikegami A, Nakauma M, Hori K, Ono T, *J Texture Stud*, **48**, 494 (2017).
192) Matsuyama S, Nakauma M, Funami T, Hori K, Ono T, *Food Hydrocoll*, **111**, 106353 (2021).
193) Nakao S, Ishihara S, Nakauma M, Funami T, *J Texture Stud*, **44**, 289 (2013).
194) Cichero JA, *Nutr J*, **12**, 54 (2013).
195) O'Keeffe ST, *BMC Geriatr*, **18**, 167 (2018).
196) Marconati M, Engmann J, Burbidge AS, Mathieu V, Souchon I, Ramaioli M, *Trends Food Sci Technol*, **86**, 281 (2019).
197) Steele CM, Alsanei WA, Ayanikalath S, Barbon CE, Chen J, Cichero JA, Coutts K, Dantas RO, Duivestein J, Giosa L, Hanson B, Lam P, Lecko C, Leigh C, Nagy A, Namasivayam AM, Nascimento WV, Odendaal I, Smith CH, Wang H, *Dysphagia*, **30**, 2 (2015).
198) Ortega O, Bolivar-Prados M, Arreola V, Nascimento WV, Tomsen N, Gallegos C, Brito-de La Fuente E, Clave P, *Nutrients*, **12**, 1873 (2020).
199) Nishinari K, Takemasa M, Su L, Michiwaki Y, Mizunuma H, Ogoshi H, *Food Hydrocoll*, **25**, 1737 (2011).
200) Nishinari K, Turcanu M, Nakauma M, Fang Y, *NPJ Sci Food*, **3**, 5 (2019).
201) Fernández Farrés I, Norton IT, *Food Hydrocoll*, **40**, 76 (2014).

202) Garrec DA, Frasch-Melnik S, Henry JV, Spyropoulos F, Norton IT, *Faraday Discuss*, **158**, 37 (2012).
203) Norton IT, Smith CG, Frith WJ, Foster TJ, in "*Hydrocolloids. Part 2*", Nishinari K (Ed), 219 (2000), Elsevier, Amsterdam.
204) Zhang K, Dai M, Yang C, Nishinari K, Fang Y, Ni X, Huang W, Dou Z, *Food Hydrocoll*, **135**, 108095 (2023).
205) Ghebremedhin M, Seiffert S, Vilgis TA, *Curr Res Food Sci*, **4**, 436 (2021).
206) Nishinari K, Fang Y, *Food Structure*, **13**, 24 (2017).
207) Takahashi R, Hirashima M, Tanida Y, Nishinari K, *Nippon Shokuhin Kagaku Kogaku Kaishi (J Jpn Soc Food Sci Technol)*, **56**, 591 (2009).
208) Barnes H, "*A Handbook of Elementary Rheology*", University of Wales Institute of Non-Newtonian Fluid Mechanics, Aberystwyth, Wales, (2000).
209) Nishinari K, in "*Food Hydrocolloids: Functionalities and Applications*", Fang Y, Zhang H, Nishinari K (Eds), 75 (2021), Springer Nature, Singapore.
210) Nishinari K, Fang Y, *Food Hydrocoll*, **112**, 106110 (2021).
211) Clasen C, Kulicke WM, *Prog Polym Sci*, **26**, 1839 (2001).
212) Cheng Y, Prud'homme RK, *Biomacromolecules*, **1**, 782 (2000).
213) Barnes HA, 9.2.1 The Cross model in "*A handbook of elementary rheology*". University of Wales Institute of Non-Newtonian Fluid Mechanics, Aberystwyth, Wales, (2000).
214) Risica D, Barbetta A, Vischetti L, Cametti C, Dentini M, *Polymer*, **51**, 1972 (2010).
215) Kongjaroen A, Methacanon P, Gamonpilas C, *J Food Eng*, **316**, 110820 (2022).
216) Morris ER, in "*Food Hydrocolloids: Structures, Properties and Functions*", Nishinari K, Doi E (Eds), 201 (1994), Springer, Boston, MA.
217) Smith CH, Logemann JA, Burghardt WR, Zecker SG, Rademaker AW, *Dysphagia*, **21**, 209 (2006).
218) Christensen CM, Casper LM, *J Food Sci*, **52**, 445 (1987).
219) Deblais A, Hollander ED, Boucon C, Blok AE, Veltkamp B, Voudouris P, Versluis P, Kim HJ, Mellema M, Stieger M, Bonn D, Velikov KP, *Nat Commun*, **12**, 6328 (2021).
220) Blok AE, Bolhuis DP, Kibbelaar HVM, Bonn D, Velikov KP, Stieger M, *Food Hydrocoll*, **121**, 107052 (2021).
221) Yoshida T, Tasaka Y, Ohie K, Murai Y, *Nihon Reoroji Gakkaishi (J Soc Rheol Jpn)*, **50**, 3 (2022).
222) Tasaka Y, Yoshida T, Murai Y, *Nagare (J Jpn Soc Fluid Mechanicss)*, **38**, 283 (2019).
223) Yoshida T, Tasaka Y, Fischer P, *Phys Fluids*, **31**, 113101 (2019).
224) Benzi R, Divoux T, Barentin C, Manneville S, Sbragaglia M, Toschi F, *Phys Rev Lett*, **127**, 148003 (2021).
225) Divoux T, Fardin MA, Manneville S, Lerouge S, *Annu Rev Fluid Mechanics*, **48**, 81 (2016).
226) Yoshida T, Tasaka Y, Murai Y, *J Rheol*, **61**, 537 (2017).
227) Ohie K, Yoshida T, Tasaka Y, Murai Y, *Ind Eng Chem Res*, **61**, 18157 (2022).
228) Wei Y, Guo Y, Li R, Ma A, Zhang H, *Food Hydrocoll*, **110**, 106198 (2021).
229) Bonn D, Denn MM, Berthier L, Divoux T, Manneville S, *Rev Modern Phys,* **89**, 035005 (2017).
230) Barnes HA, *J Non-Newtonian Fluid Mechanics*, **81**, 133 (1999).
231) Møller PCF, Fall A, Bonn D, *EPL (Europhysics Letters)*, **87**, 38004 (2009).
232) Reiner M, *Physics Today*, **17**, 62 (1964).
233) Mewis J, Wagner NJ, *Adv Colloid Interface Sci*, **147-148**, 214 (2009).
234) Dinkgreve M, Paredes J, Denn MM, Bonn D, *J Non-Newtonian Fluid Mechanics*, **238**, 233 (2016).
235) Barnes HA, *J Non-Newtonian Fluid Mechanics*, **70**, 1 (1997).
236) Larson RG, Wei Y, *J Rheol*, **63**, 477 (2019).
237) Wei Y, Li R, Zhang H, *Phys Fluids*, **34**, 123107 (2022).
238) Brenner T, Matsukawa S, Nishinari K, Johannsson R, *J Non-Newtonian Fluid Mechanics*, **196**, 1 (2013).
239) Brenner T, Nicolai T, Johannsson R, *Food Res Int*, **42**, 915 (2009).
240) Lindström SB, Kodger TE, Sprakel J, Weitz DA, *Soft Matter*, **8**, 3657 (2012).
241) Sprakel J, Lindstrom SB, Kodger TE, Weitz DA, *Phys Rev Lett*, **106**, 248303 (2011).
242) Yang K, Liu Z, Wang J, Yu W, *J Rheol*, **62**, 89 (2018).
243) Fang Y, Takahashi R, Nishinari K, *Biopolymers*, **74**, 302 (2004).
244) Grassi M, *Carbohydr Polym*, **29**, 169 (1996).
245) Li X, Fang Y, Zhang H, Nishinari K, Al-Assaf S, Phillips GO, *Food Hydrocoll*, **25**, 293 (2011).
246) Toker OS, Karasu S, Yilmaz MT, Karaman S, *Food Res Int*, **70**, 125 (2015).
247) Li R, Wang P, Ma A, Zhang H, *Food Hydrocoll*, **144**, 109018 (2023).